SOVIET PHYSICS USPEKHI VOLUME 8, NUMBER 1 JULY-AUGUST, 1965
539.893

USE OF SHOCK WAVES IN HIGH-PRESSURE PHYSICS

L. V. AL'TSHULER

Usp. Fiz. Nauk 85, 197-258 (February, 1965)

INTRODUCTION

THE inclusion of powerful shock waves in the research arsenal of modern physics has made pressures on the order of hundreds of thousands and millions of atmospheres an object of laboratory experiments. The effect of similar and even higher pressures is experienced in the world surrounding us in the depth of the earth, in the center of the sun, and inside other cosmic bodies of large mass. The pressures on the boundary of the earth's core, at a distance of 2,900 km from its surface, reach 1.4 million atm. In the center of the earth they are equal to 3.5 million atm, while in the center of the sun they amount to a billion atmospheres and in white dwarfs 100 quadrillion atm. The temperatures amount to several thousand degrees in the earth's core, and tens of millions of degrees in stars. Higher and higher pressures and temperatures are gradually being produced artificially and used to solve a great variety of scientific and technical problems. In many cases man-made processes duplicate for a short duration conditions that exist in central regions of stars.

The most accessible for theoretical study are extreme states of matter at very large compressions and very high temperatures. We know well the thermodynamic characteristics of a plasma consisting of a mixture of nuclei and electrons under conditions of total temperature ionization.

The properties of a degenerate electron gas filling a volume uniformly are of elementary simplicity at pressures on the order of $5 \times 10^8 Z^{10/3}$ atm, (Z—atomic number)[1]. At lower pressures, the distribution of electrons in the potential field of nuclei is described by the Thomas-Fermi-Dirac quantum-statistical theory. Its most accurate variant, which takes into account not only the exchange but also the so-called quantum correction, was developed in the Soviet Union by Kirzhnits [2] and by Kalitkin [3].

It is difficult to establish exactly the limits of applicability of statistical representations. A pressure of several hundred million atmospheres is apparently enough to "crumple" the outer electron shells of the atoms and to bring the densities on the periphery of the electron clouds in correspondence with the laws of quantum statistical distribution; on the other hand, within the first several million atmospheres, the compression curves are governed wholly by the individual structures of the electron shells of elements or compounds, and their properties depend on the character and specific features of the chemical bonds.

Pressures modify or break these bonds, causing the formation of new and denser crystal modifications with a higher coordination of the atoms and with radically altered physical and chemical properties. For insulators and semiconductors, the end result of application of pressure is always a transition to the metallic state.

A sufficiently exact theoretical analysis of all these phenomena, together with calculation of the compression curves, has met so far with great difficulties.

A major step forward towards overcoming these difficulties was recently made by Gandel'man et al.[4,5], who calculated in the spherical-cell approximation the energy spectra of several metals under different degrees of compression.

Until recently the pressures experimentally investigated with stationary laboratory equipment did not exceed the 100,000 atm attained in the classical work of Bridgman [6,7] in the early Forties. Recently,

Vereshchagin and his co-workers [8,9] in the Soviet Union and many foreign scientists [10,11] made noticeable progress and succeeded in obtaining critical shear stresses and critical conductivity and in observing the appearance of new phases at several hundred thousand atmospheres. A new accomplishment was the possibility of taking x-ray structural photographs under pressure [12-14].

In spite of the appreciable progress made on the pressure scale, until recently a great gap remained between the attained experimental level and the region of compressions which can be reliably calculated theoretically.

The development of dynamic techniques in high-pressure physics has made it possible to make rapid progress and greatly reduce an uninvestigated region of particular interest to solid and liquid state physics, geophysics, and planetary astronomy.

Dynamic methods are based on the registration of kinematic parameters of shock waves—their wave and mass velocities, which determine the pressures, densities, and energies of shock compression.

In experiments with shock waves, measurements are also made of the isentropic elasticity of strongly compressed substances, of the conductivity induced by compression and heating in the case of dielectrics, and of the temperatures behind the shock-wave front in the case of transparent substances.

The realization of dynamic methods is not connected with the use of presses and piezometric bombs, and is not limited by the strength of the materials used for their production. When experiments are carried out in samples in which shock waves move, high pressures are retained over short time intervals because of the inertia of the material, owing to the finite velocity of propagation of dilatation waves. Extensive use of shock waves in high pressure physics began after the Second World War. In the present review we give the main results obtained since then in the study of explosives and of equations of state of superdense gases, metals, and ionic and covalent crystals by dynamic methods. The article considers also problems of phase transformations in shock waves, the use of the resultant data in geophysics, and problems of dynamic strength of metals and of shock-induced conductivity.

To limit the size and restrict the topic of the review, problems of pulsed x-ray diffraction studies and the investigation of optical properties of shock-compressed substances are barely touched upon. The most noticeable results accomplished in these promising trends, each of which can serve as a subject of a separate review, were obtained by Tsukerman [15-19], Schaafs [20] and Schall (see [21]), in the field of microsecond x-ray photography, and by Sobolev and Belyaev [22], Gibson [23], Model' [24], Zel'dovich, Kormer, and Sinitsyn [25], and Voskoboĭnikov and Apin [26], in the question of the registration of temperatures behind the front of shock waves and detonation waves.

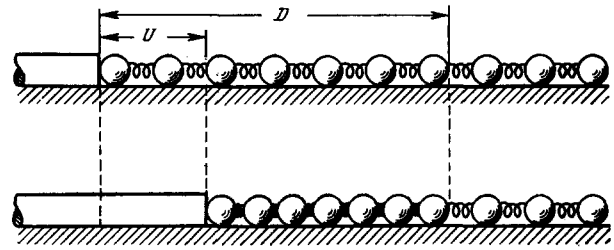

FIG. 1. One dimensional model of propagation of shock wave in an elastic medium.

In addition to the present work, earlier reviews of the dynamic trend are presented in the "Physics of Shock Waves" of Zel'dovich and Raĭzer [27], and in the survey articles of Rice, McQueen, and Walsh [28], Alder [29], Duvall [30], and Jacobs [21]. The gas-dynamic principles of the theory of shock waves are developed in the books of Courant and Friedrichs [31], Zel'dovich [32], and Baum, Stanyukovich, and Shekhter [33]. The presence of these reviews and monographs has enabled the author in many cases to forego references to the original sources.

1. SHOCK ADIABATS AND THEIR EXPERIMENTAL REGISTRATION

The propagation of a shock wave in a substance can be visualized with the aid of a series of spheres which are elastically coupled to one another (Fig. 1). The rate of displacement of the spheres—the "mass" velocity of the substance U—is equal in our experiment to the velocity of a piston which causes the spheres to move. This velocity is always lower than the velocity D of the perturbation boundary separating the resting and separated spheres from those moving and gathered into a more compact mass.

From the conditions for the conservation of matter, momentum, and energy it follows that

$$\frac{D}{D-U}=\frac{v_0}{v}=\sigma, \tag{1a}$$

$$\frac{DU}{v_0}=P-P_0, \tag{1b}$$

$$\frac{1}{2}U^2=E-E_0=\frac{1}{2}(P+P_0)(v_0-v), \tag{1c}$$

where P is the pressure behind the wave front, P_0 the pressure ahead of the front, v and v_0 the specific volume behind and before the wave fronts, E and E_0 the specific internal energies in the same states, and σ the degree of relative compression of the substance.

The conservation equations have an intuitive geometrical interpretation. As follows from the first two equations, when $P_0 = 0$ we have

$$D^2=v_0^2\frac{P}{v_0-v}, \tag{2a}$$

$$U^2=P(v_0-v). \tag{2b}$$

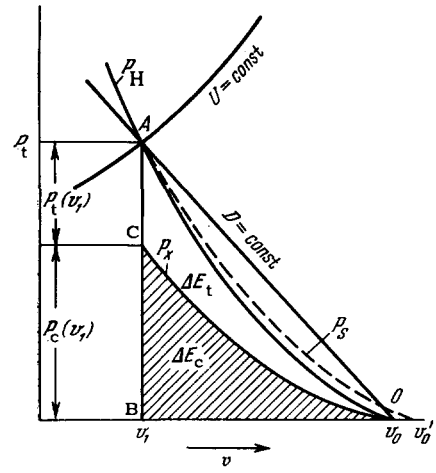

FIG. 2. P-v diagram of shock compression. P_H – shock adiabat of compression – the Hugoniot adiabat; P_S – isentrope of expansion of shock-compressed substance; P_c – curve of "cold" compression at T = 0°K – zero isotherm.

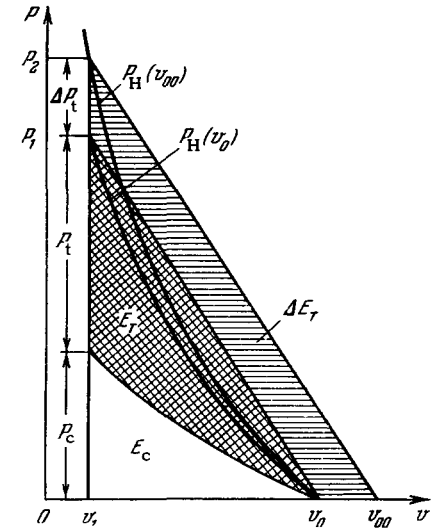

FIG. 3. Shock adiabats $P_H(v_0, v)$ and $P_H(v_{00})$ of solid and porous material.

Any set of definite values of D and U corresponds on the P – v diagram (Fig. 2) to a straight line B = const and a hyperbola U = const.

The intersection of the line and of the hyperbola fixes the state of the shock compression with coordinates P_1 and v_1. The aggregate of the states which arise when the substance is compressed by shock waves of different intensity determines the position of the shock-compression curve—the Hugoniot adiabat $P_H(v_0, v)$.

Measurements of the quantities D and U are equivalent to direct determination of the pressures and specific volumes, as follows also directly from the system of Eqs. (1). Dynamic methods of research are based on this equivalence.

As follows from (1c), the total increase ΔE in internal energy is equal to the area of the triangle OAB. This increment consists of an "elastic" component ΔE_c, lying between the volume axis and the "cold" compression curve $P_c(v)$, and the thermal energy ΔE_t, represented by the curvilinear triangle OAC. Inasmuch as $\Delta E_c < \Delta E$, the shock-compression process is accompanied by heating of the substance and by an increase in its entropy, which in turn leads to the appearance of a thermal pressure component P_t. With increasing wave amplitude, the thermal energy and the thermal pressure of shock compression increase progressively.

The initial section of the dynamic adiabat is determined essentially by the compression curve $P_c(v)$ at absolute zero temperature (the zero isotherm). To the contrary, the position of its upper branch depends on the thermodynamic characteristics of the compressed medium.

An idea of the behavior of the dynamic adiabat can be obtained by substituting Eq. (1c) into the simplest equation of state of a solid [34]

$$P - P_c = \frac{\gamma}{v}(E - E_c), \tag{3}$$

where

$$E_c = -\int_0^{v_0} P_x\, dv.$$

The resultant expression

$$Pv = \frac{(h-1)P_c v - 2(E_c - E_0)}{h - (v_0/v)} \tag{4}$$

becomes infinite when the relative compression of the medium $\sigma = v_0/v$ reaches a limiting value $h = 1 + (2/\gamma)$. As follows from (3), the parameter γ relates the thermal pressure with the density of thermal energy. In the general case the coefficient γ is a complicated function of the volume and of the temperature. In metals, the values of h and γ under normal conditions are close to 2. If their thermal characteristics were to remain constant, the shock adiabats would approach asymptotically the limiting value $\sigma = 2$ ($v = v_0/2$). Since the coefficient γ decreases with density and temperature, the actually attained compressions can greatly exceed the indicated value.

Obviously, knowledge of the dynamic adiabats is very important both for the determination of the zero isotherms and for obtaining valuable information on the thermodynamic parameters of the investigated substances at high pressures and temperatures.

An important role in the solution of the latter problem is played by shock compression of porous bodies of reduced initial density, proposed as a research method by Zel'dovich [35,27]. As can be seen from Fig. 3, the larger deformation of porous samples with initial volume $v_{00} = mv_0$ is accompanied by a considerable increase in the thermal energy and a corresponding increase in the thermal pressure.

As a result, the "porous" adiabats always lie

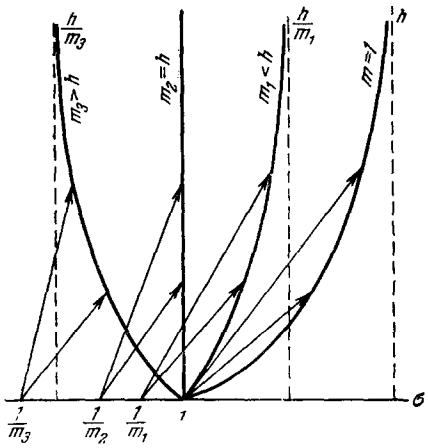

FIG. 4. Shock adiabats of samples with different initial porosity $m_3 > h$, $m_2 = h$, $m_1 < h$, and $m = 1$. The initial relative densities are $1/m_3$, $1/m_2$, $1/m_1$ and 1; the limiting compressions are h/m_3, h/m_2, h/m_1 and h and are denoted by dashed vertical lines; for $m_2 = h$ the vertical line and the dynamic adiabat coincide with the ordinate axis.

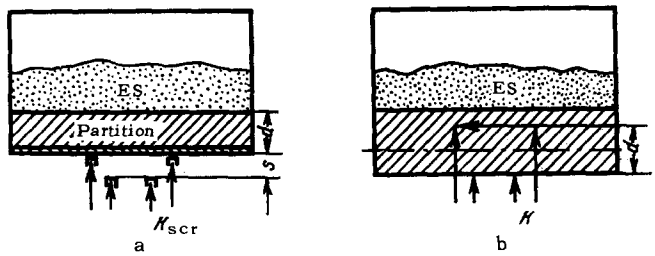

FIG. 5. Scheme for measuring: a) mass and b) wave velocities in partitions. S – for measurement of the velocity of the free boundary; d – base of measurement of wave velocity; K – contact making pickups; K_{scr} – pickup with a screen protecting the contacts from prior closing by the shock wave in air.

above the "solid" ones. Their equation for constant γ is similar to (4), in which v_0 in the denominator is replaced by v_{00}. Obviously, in this case the pressures become infinite at specific volumes $v = m(v_0/h)$—at the limiting degrees of compression $\sigma = h/m$.

A schematic diagram of the compression of porous samples, taken from [87], under the assumption that h is constant, is shown in Fig. 4. The abscissas show the degrees of compression and the ordinates the pressures.

If the porosity m is smaller than h, shock compression increases the density. When $m > h$, the final density of the medium decreases with increasing pressure, remaining always smaller than the normal density of the solid substance. If $m = h$, any pressure reduces a porous medium only to the normal density of the solid state. In this case the shock adiabat is represented by a vertical line coinciding with the pressure axis. The configuration of porous adiabats is a very sensitive indicator of the thermodynamic characteristics of the medium.

Comparison of the adiabats of the solid substances and of the substance which has low porosity in the initial state makes it possible to determine the parameter γ experimentally. As follows from Fig. 3, for compression to an equal volume, the difference in the thermal pressures ΔP_t is explained by the difference in the heat energies

$$\Delta E_t = \frac{1}{2}[P_2(v_{00} - v) - P_1(v_0 - v_1)].$$

The sought value of $\gamma(v_1)$ is obtained from the ratio $v_1 \Delta P_t(v_1)/\Delta E_t(v_1)$.

The development of dynamic methods started independently in the USA in 1944 by Goranson (see [21,28]) and in the Soviet Union in 1947–48 by the author of this review, Tsukerman, Krupnikov, and Kormer (see [36,38]). Research of similar character was undertaken by Baum, Stanyukovich, and Shekhter [33].

To carry out measurements with the aid of shock waves, the experimenters had to determine their wave and mass velocities. Registration of wave velocities with pickups placed on the path of the wave motion does not entail any difficulty in principle. Direct observation of mass velocity, on the other hand, is in most cases impossible. Up to the relatively low pressures of some several hundred thousand atmospheres, which are produced when detonation waves are reflected from partitions, the mass velocities were determined from the velocity of motion of the free boundary of the partition—after the emergence of the shock wave from the latter [28,36] (Fig. 5).

Layers adjacent to the free surface go into motion under the influence of two different processes—shock transition from the state $P_0 = 0$, v_0 into the state P_1, v_1 (see Fig. 2) and subsequent isentropic expansion in the reflected rarefaction wave to a state $P = 0$, $v_0' > v_0$.

In spite of the difference in the processes, we can assume with good approximation that so long as $U \ll D$

$$W = 2U. \tag{5}$$

The registration of higher pressures calls for introducing calculated corrections to take into account the deviation from the doubling law.

A method whose starting premises are perfectly rigorous is the "deceleration" method developed in the Soviet Union by the authors of [36] in the late Forties to obtain and to investigate the pressure of several million atmospheres. The experimentally measured quantities in the decleration method are the velocity W_s of a striker accelerated by the explosion products until it strikes a target of the investigated material, and the velocity D of the shock wave in the target (Fig. 6).

The deceleration of the striker by the investigated partition produces two waves of equal pressure, propagating in both sides of the collision surface. The velocity U of this surface after the shock is the

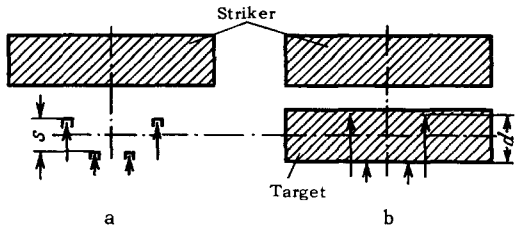

FIG 6. Scheme for the measurement of mass and wave velocities by the deceleration method. a) – Registration with screened pickups of the striker velocity; b) – registration of wave velocities in the target

mass velocity behind the wave front. The jump in velocities on the front of the wave is equal to $W_S - U$ in the striker and to U in the target. If the target and the striker are made of the same material and the striker does not experience any appreciable heating during the course of its acceleration, then $W_S - U = U$, and consequently

$$U = \frac{1}{2} W_s. \qquad (6)$$

The main parameters of the shock wave and of the target are obtained by substituting U and the wave velocity D in the conservation laws (1).

Expression (6) is outwardly similar to (5). In the former case, however, the partition acquires velocity by two essentially different processes—shock compression and subsequent dilatation, which give approximately identical velocity increases only for relatively weak shock waves. To the contrary, in the deceleration method the condition that the velocity is reduced to ½ after the impact is satisfied perfectly rigorously for arbitrary large velocities of motion and for arbitrary pressures and temperatures of the shock compression.

When different bodies collide, the velocity jumps in the target and in the striker are not equal. This difficulty is overcome by making the striking body of

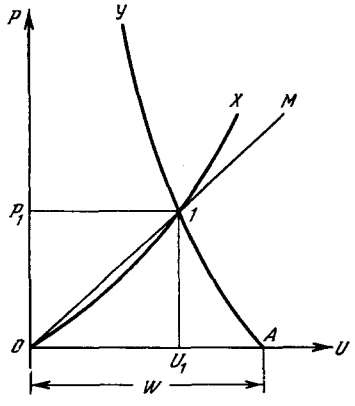

FIG. 7. P-U diagram of shock deceleration. AY – Hugoniot adiabat of the decelerating striker; OM – wave ray of the target; 1 – state of shock compression; OX – shock adiabat of target made of the investigated substance.

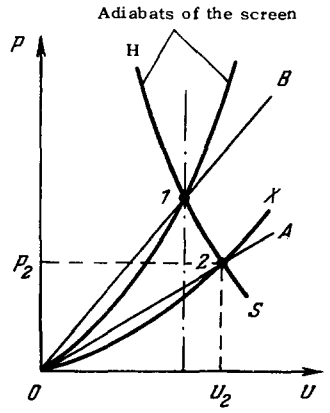

FIG. 8. Determination of the shock-compression parameters by the reflection method. 1 – State of shock compression in the screen: 1 – S – isentrope of expansion of the screen material; 1 – H – shock adiabat of compression of the screen from state 1; OB – wave ray $P = \rho_{0scr} D_{scr}$ and of the screen material; OA – wave ray $P = \rho_{0c} D_c$ and of the investigated material; 2 – state of shock compression of the sample; OX – investigated adiabat.

a material having a known dynamic adiabat that relates functionally the shock compression pressure with the velocity jump $W_S - U$. On the pressure-velocity diagram (Fig. 7), the dynamic adiabat for the deceleration of the striker is represented by curve AY, which passes at a distance W_S from the origin. Measurement of the wave velocity D fixes the position of the wave ray OM satisfying the equation $P = \rho_0 DU$ (ρ_0—initial density of the target material).

What is actually realized is state 1 at the intersection of the striker adiabat AY and the straight line OM. The coordinates of the intersection point determine the pressure P_1 and the velocity U_1, and from these values, in accordance with Eq. (1a), also the density of shock compression $\rho_1 = 1/v_1$.

In many cases [28,38] it is more convenient to apply the shock wave to the investigated substances through a screen made of material with an already known Hugoniot adiabat. The experimentally measured quantities in this case are the velocities of the shock waves in the screen and in the investigated samples (the "reflection" method).

On the pressure-velocity diagram (Fig. 8), the possible states of shock compression of the screen and of the sample, for fixed velocities of the shock waves, correspond to the wave lines OB and OA. State 1 of the screen is determined by where its wave line crosses its Hugoniot adiabat. State 2 of the sample lies in turn where the screen expansion isentrope or its deceleration adiabat crosses the wave ray of the sample OA. If the points 1 and 2 are not too far from each other, then curve 1-2 is approximated with high accuracy by the mirror reflection of the screen adiabat relative to the straight line passing through the initial state 1.

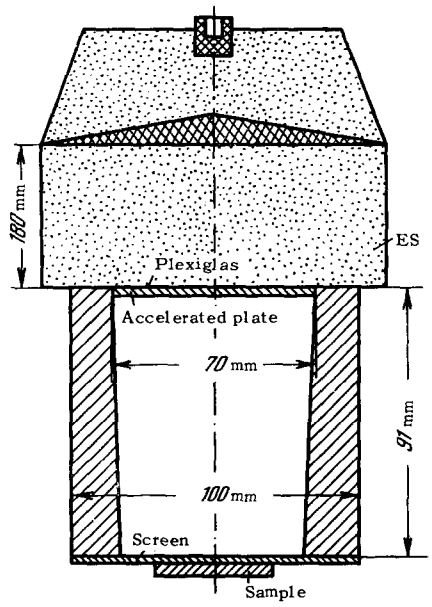

FIG. 9. Acceleration of thin steel discs by explosion products. ES – explosive charge.

One of the devices [39] intended for investigations by the braking method is shown in Fig. 9.

A 1-1/2 mm steel disc attached to the charge is accelerated to 5600 m/sec by expanding explosion products and passes through a lead nozzle over a distance of 90 mm length.

To minimize the heating of the striker, the accelerated disc is separated from the charge by a thin layer of Plexiglas or by an air gap of 5–6 mm, to ensure a smooth buildup of the explosive-substance pressures. At the end of the path, the disc strikes a screen on which are placed the investigated samples. Analogous systems were described by McQueen and Marsh [40].

In the investigations of the British scientists Morris and Skidmore [41], reported in 1962, the striker was a thin steel shell of a hemispherical cumulative charge, striking synchronously the investigated sample, which in turn was made in the form of a spherical segment with outside radius 76 mm. The results of the measurements of the wave velocities were extrapolated to the external surface of the segment, where they were compared with the velocity of motion of the shell at the instant it struck the segment. In [41] this velocity amounted to ~9 km/sec. In the work of the Soviet scientists, the striker velocities reached ~9 km/sec in [36-39], and ~14 km/sec in [42,43] and others.

The rates of displacement of the shock fronts, partitions, and strikers are usually determined with electric-contact pickups introduced in the body of the sample (Figs. 5b and 6b), or placed along the path of motion of the partitions and the strikers (Figs. 5a and 6a). At bases of 5 mm and velocities

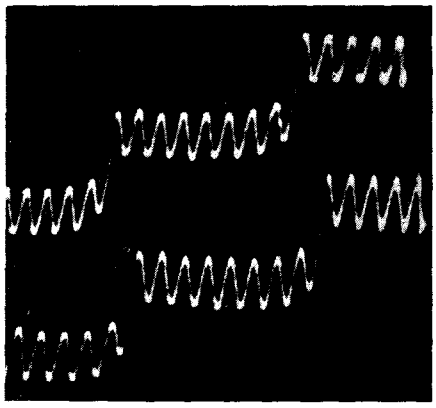

FIG. 10. Oscillogram recording the time between the closings of pickup contacts. The period of the scale sinusoid is 5×10^{-8} sec.

5–10 km/sec, the measured time intervals amount to $(0.5–1.0) \times 10^{-6}$ sec. Modern high speed oscilloscopes can record these intervals with an accuracy of ~1% (Fig. 10).

In the Soviet Union, the electric-constant procedure was developed in 1947–1948 by Tsukerman, Krupnikov, Etingof, and Lebedev, with the author of this review participating [36]. In the USA, the procedure was developed independently somewhat earlier by Goranson [44], Mallory [45], and others. [28]

Another method of registering very fast processes is based on recording light signals on rotating-mirror cameras. The rate of motion of the beam on the film in such instruments reaches 4–6 km/sec [46].

In experimental gasdynamical practice, the use of photographic methods for the measurement of detonation speeds is traditional. They found extensive application in the Soviet Union and in the USA from the very beginning also in the study of strong shock waves—for the measurement of wave and mass velocities and the speeds of sound in compressed matter, for recording wave collisions, and for continuous observation of the trajectories of surface motion. Some examples of the use of optical recording by Soviet researchers are presented in Secs. 5 and 6. Photography with a slit photochronograph was used by Walsh and Christian [47,28] as the principal experimental method. A schematic diagram of the experimental block and of the photochronogram (from [28]) are shown in Fig. 11.

The moving image of the slot through which the photograph is taken records on the film the successive passage of the shock waves through the gaps on the boundary between transparent Plexiglas blocks and the screen with the samples, and also the striking of the sample against the partition. Glow is initiated when the shock wave enters the gaps and stops several nanoseconds later when the shock wave enters into the plexiglas plates, which lose their transparency upon impact.

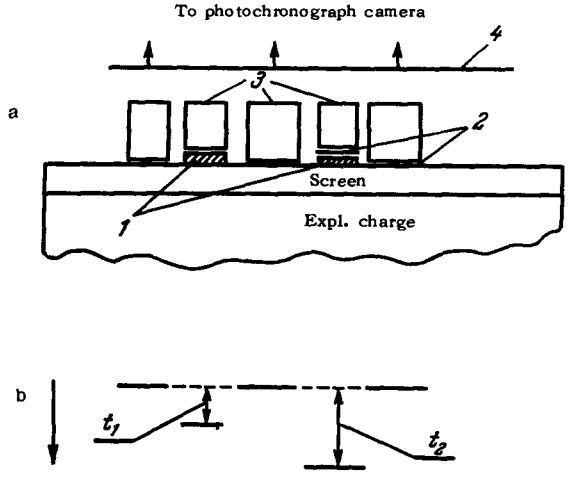

FIG. 11. Photochronographic measurements of wave and mass velocities[28]. a) Diagram of the experiment: 1 – investigated samples; 2 – gaps filled with argon, glowing when the shock wave passes; 3 – transparent blocks of organic glass; 4 – screen with slit. b) Scheme of photochronogram: t_1 – time of passage of shock wave through the sample; t_2 – combined time of passage of shock wave over the sample and motion of its free surface; the arrow indicates the direction of displacement of the image of the slit over the film.

With increasing shock-wave amplitude, regardless of the registration method used, the difficulties of experimentally determining the pressure and the compression by dynamic means increase progressively. The reasons lie in the deterioration of the symmetry of motion of the strikers and of the shock waves, and in the decrease in the recorded time intervals. There is a particularly strong decrease in the accuracy with which the density is determined, since its calculation by formula (1a) involves differences between the wave and mass velocities. At the same time, the theoretical analysis of the properties of the substances becomes easier with increasing degree of compression.

The demarkation line between the region of advantageous application of gasdynamic experiments apparently lies at pressures of 10—15 million atmospheres and at densities 3—3.5 times normal. At the present time this limit has almost been reached for some substances.

2. METHODS OF OBTAINING SEMIEMPIRICAL EQUATIONS OF STATE

The results of experiments with shock waves give enough material to construct semiempirical equations of state, describing the behavior of solids and liquids at high pressures and temperatures.

The properties of matter under these conditions are determined by the forces of interaction at absolute zero temperature, by the thermal vibrations of the atoms or ions, and by the thermal excitation of the electrons.

To determine the cold-compression curves from the experimental results of dynamic experiments, and to derive the equations of state of compressed matter, it is necessary to resolve the shock pressures into thermal and cold components. To solve this problem it is necessary first to introduce into consideration methods for describing the thermal properties of atoms.

If the temperatures are not too high, the atoms of a solid or a liquid (we shall not distinguish here between these phases) execute in the main vibrations about their equilibrium positions. Their displacement in space, by jumping over into an interstice or into some other vacant site, calls for overcoming potential barriers of height on the order of one or several electron volts at normal densities [27]. This means that the vibration energy of the order of kT per atom is comparable with the height of the potential barrier at temperatures on the order of tens of thousands of degrees. When the material is compressed, the increase in the repulsion forces greatly raises the heights of the potential barriers. The free displacements of the particles become even more difficult then, and their motion remains limited to the space of their own cells. Under these conditions, the motion retains the properties of harmonic oscillations over a wide temperature interval, including also the state arising when "continuous" samples are shock-compressed.

The thermal energy of a "classical" ensemble of oscillators is $E_{t.eq} = 3\,RT/\bar{A}$ (the Dulong and Petit law), and the thermal pressure is

$$P_t = \frac{\gamma_{eq}}{v}\frac{3R}{\bar{A}}T \quad \text{with} \quad \gamma_{eq} = \frac{d\ln\bar{\omega}}{d\ln v}$$

(the Gruneisen law). In these expressions R is the gas constant, $\bar{A}$ the average atomic weight, and $\bar{\omega}$ the average frequency. Taking into account the quantum effects, which become significant at temperatures less than or equal to the Debye temperature θ, the equation of state in the Mie-Gruneisen form is

$$\left.\begin{aligned} P &= P_c + \frac{\gamma_{eq}}{v}\frac{3R}{\bar{A}}TD\left(\frac{\theta}{T}\right), \\ E &= E_c + \frac{3R}{\bar{A}}TD\left(\frac{\theta}{T}\right), \end{aligned}\right\} \qquad (7)$$

where $D(\theta/T)$—Debye function, equal to unity when $T \gg \theta$. Its caloric form, obtained by eliminating from the system (7) the temperature terms, is given by (3). The initial values of $\gamma(v_0)$ under normal conditions are obtained from the thermodynamic identity [34] $\gamma_{eq} = 3\alpha/\rho_0 c_V \kappa$, where α is the coefficient of linear expansion, κ—the coefficient of compressibility, ρ_0 the density under normal conditions, and c_V the specific heat at constant volume.

Further change in $\gamma(v)$ with volume is estimated either experimentally, for example from the position of the adiabat of porous samples [36,29] (see Sec. 1), or with the aid of some model representation, which

gives the dependence of the average frequency on the volume. The second method has been most widely used. According to Slater [48] and Landau [49], all the frequencies change in proportion to the speed of sound $C_c = v(-dP_c/dv)^{1/2}$ and are inversely proportional to the interatomic distance $r \sim v^{-1/3}$. Under these assumptions

$$\omega \sim v^{\frac{2}{3}}\left(-\frac{d}{dv}P_c\right)^{\frac{1}{2}}.$$

According to Dugdall and McDonald [50]

$$\omega \sim v^{\frac{1}{3}}\left[-\frac{d}{dv}(P_c v^{\frac{2}{3}})\right]^{\frac{1}{2}}.$$

According to Zubarev and Vashchenko [51], for particles which vibrate in a spherically-symmetrical field of their neighbors (the free-volume theory)[52],

$$\omega \sim -\left[\frac{d}{dv}(P_c v^{\frac{4}{3}})\right]^{\frac{1}{2}}.$$

All these different expressions can be represented by a single formula for the frequency

$$\omega \sim v^{\frac{2-t}{3}}\left[-\frac{d}{dv}P_c(v^{\frac{2t}{3}})\right]^{\frac{1}{2}}. \qquad (8)$$

Its logarithmic derivative with respect to the volume determines the Gruneisen coefficient

$$\gamma_{eq}(v) = -\left(\frac{2}{3}-\frac{t}{3}\right) - \frac{v}{2}\frac{\frac{d^2}{dv^2}(P_c v^{\frac{2t}{3}})}{\frac{d}{dv}(P_c v^{\frac{2t}{3}})}. \qquad (9)$$

The value t = 0 corresponds to the Landau-Slater theory, t = 1 to the Dugdall and McDonald theory, and t = 2 to the free volume theory. When $v = v_0$ we have

$$\gamma_{eq}(t=0) = \gamma_{eq}(t=1) + \frac{1}{3} = \gamma_{eq}(t=2) + \frac{2}{3}.$$

For central forces with a power-law variation in the form $P = Av^{-n}$,

$$\gamma_{eq} = \frac{1}{2} + \frac{n-1}{2}$$

does not depend on the density and is the same for all t. The limiting value of γ_{eq} for a free electron gas is $2/3$. The initial values of $\gamma_{eq}(v_0)$ for most ionic crystals and metals lie in the range from 1.5 to 2.5. As was shown in [28] and [53], for most cases a value t = 1 holds for metals and t = 2 for ionic crystals.

To determine the functions $\gamma(v)$ and $P_c(v)$ and the shock-compression temperatures T_H it is necessary to solve simultaneously Eqs. (7) and (9), with the parameters of the experimental adiabats substituted in the left sides of (7); these parameters are the pressures P_H and energies

$$E_H = \frac{1}{2}P_H(v_0 - v) + E_0.$$

To describe the high temperature states which are produced, in particular, under shock compression of porous samples, an account of the anharmonicity of the thermal vibrations of the atoms and ions is a must. According to Kormer and Urlin [54,55], it is possible to use for this purpose the following interpolation formula for the frequency

$$\omega \sim \left[-v^{\frac{2(2-t)}{3}}\frac{d}{dv}(P_c v^{\frac{2t}{3}}) + l\frac{RT}{\bar{A}}v^{-\frac{2}{3}}\right]^{\frac{1}{2}}, \qquad (10)$$

which differs from (8) in the presence of a second temperature term. Substitution of (10) in the expression for the free energy $F = RT \ln(\hbar\bar{\omega}/kT)$ at low and very high temperatures leads to correct expressions for the free energy of a solid or of an ideal gas. For intermediate states, the decisive factor is the parameter l, which is found from experimental adiabats of porous samples.

In expanded form, according to [55], we have

$$\left.\begin{aligned} P &= \frac{3\gamma_{eq}+z}{1+z}\frac{RT}{v\bar{A}} + P_c, \\ E &= \frac{2+z}{1+z}\cdot\frac{3}{2}\frac{RT}{\bar{A}} + E_c, \end{aligned}\right\} \qquad (11)$$

where

$$z = \frac{lRT}{\bar{A}(c_c^2 - 2tP_x v)}, \qquad c_c^2 = -v^2\left(\frac{dP_c}{dv}\right). \qquad (11a)$$

As $z \to 0$, Eqs. (11) and (11a) become identical with the Mie-Gruneisen equations of state (7).

To calculate the properties of a compressed and strongly heated substance, we can use also the theory of free volume (t.f.v), which does not call for introducing empirical parameters such as l. This theory considers the motion of particles in cells with impermeable walls, separated from one another by infinitely high potential barriers. For compressed matter this theory is a good approximation of reality.

According to the theory of free volume [52], the statistical integral of the system contains as a factor the "free" volume of the cell

$$v_f = \int_{\Delta} e^{-\frac{\chi(\mathbf{r})-\chi(\mathbf{r}_0)}{kT}}d\mathbf{r} \qquad (12)$$

raised to the N-th power (N—number of particles). In formula (12), $\mathbf{r}$ is the running radius vector, $\mathbf{r}_0$ the radius vector of the equilibrium position at the center of the cell, $\chi(\mathbf{r})$ the potential energy of the particle, and Δ the volume of the cell.

At low temperatures, the free-volume theory describes harmonic motion with a per-unit specific heat $3R/\bar{A}$ and with a Gruneisen coefficient calculated from Eq. (9) at t = 2. At high temperatures, when kT is much larger than the average difference of the potential energies $\overline{\chi(\mathbf{r})} - \overline{\chi(\mathbf{r}_0)}$, the "free" volume v_f in (12) coincides with the geometrical volume of the cell. Under these conditions, the aggregate of the particles forms a "lattice" ideal gas, the equation of state of which is identical with the equation of state of a true ideal gas (with the exception of the entropy, which is smaller by a constant factor equal to the entropy of the permutation of the particles among the cells).

The free volume theory makes it possible, starting from the potential interaction of the particles, to find the thermodynamic functions, both for the indicated limiting cases and for the intermediate stages of the transition of the bodies into an effective gaseous state.

Practical calculations are carried out in cell theory for an idealized spherically-symmetrical strong field. In this lies the approximate character of the theory, which also fails to take into account the correlations in the movement of the atoms. Consequently, its formulas do not always lead to correct values of the Gruneisen coefficient under normal conditions. In spite of these shortcomings, the free-volume theory has found extensive use in the theory of liquids. It was used by Zubarev and Telegin [56-58] for an analysis of the dynamic experiments and to obtain with their aid the equations of state of explosion products and their components, by Al'tshuler and Pavlovskiĭ to derive the equations of state of ionic crystals [53], and by Alder and Thiel [59] to obtain the equation of state of argon.

A rise in temperature to many thousands of degrees, along with anharmonicity of the thermal vibrations of the atoms, leads to thermal excitation of the electrons, primarily in metals. Consequently, the high-temperature equation of state of a metal should include, besides the lattice components, terms that represent the thermal energy and the thermal pressure of the electron gas.

Postponing a more detailed examination of this question to Sec. 4, we present here an expanded equation of state of metals, after [39,60], supplemented with thermal electronic terms:

$$\left.\begin{aligned} P &= P_c + \frac{\gamma_{eq}}{v}\frac{3RT}{A} D\left(\frac{\theta}{T}\right) + \frac{\gamma_e}{v}\frac{\beta T^2}{2}, \\ E &= E_c + \frac{3RT}{A} D\left(\frac{\theta}{T}\right) + \frac{\beta T^2}{2}. \end{aligned}\right\} \qquad (13)$$

Here $\beta = \beta_0(v/v_0)$ is the coefficient of electronic specific heat, β_0 is its experimental value at $v = v_0$, and γ_e is the electronic analog of the Gruneisen coefficient, expressing the ratio of the thermal pressure of the electrons to the density of their thermal energy.

In those cases when anharmonicity becomes significant, the lattice terms should be calculated from (11) or with the aid of the theory of the free volume.

In the first investigation [28,39,40], the functions T_H, $P_c(v)$, and $\gamma_{eq}(v)$ were determined from the experimental shock adiabats by numerical methods by simultaneously solving (7) or (13) with the differential equation (9). This method, which is indirectly connected with double differentiation of the empirical shock-compression curve, does not lead, at low degrees of compression, to unique values of $\gamma_{eq}(v)$ and does not yield analytic expressions for $P_c(v)$ which would be convenient for extrapolation. Because of this, Kormer and Urlin [61,60] obtained for $P_c(v)$ an analytic expression in the form of a series

$$P_c(v) = \sum_{n=1}^{7} a_i \delta^{i+\frac{1}{3}}, \qquad \delta = \frac{v_{0k}}{v}; \qquad (14)$$

where v_{0k} is the specific volume at $P = 0$ and $T = 0°K$.

The coefficients of the series were found by using the characteristics of the material under normal conditions [binding energy, density, compressibility, value of $\gamma_{eq}(v_0)$], the coordinates of two points of the curve $P_c(v)$ in the quantum-statistical region of pressures, and one of the points of the dynamic adiabat.

In other investigations (Davydov [66], Zharkov [62], Al'tshuler, Pavlovskiĭ, and Kuleshova [63,53], Al'tshuler, Bakanova, and Trunin [42]) the pressures and energies of cold compression were expressed by means of formulas borrowed from the theory of ionic crystals [64]:

$$\left.\begin{aligned} P_c(\delta) &= Q[\delta^{\frac{2}{3}}\exp\{q(1-\delta^{-\frac{1}{3}})\} - \delta^{\frac{4}{3}}], \\ E_c(\delta) &= 3Qv_{0k}[q^{-1}\exp\{q(1-\delta^{-\frac{1}{3}})\} - \delta^{\frac{1}{3}}]. \end{aligned}\right\} \qquad (15)$$

For ionic compounds, the first terms in (15) are determined by the Born-Mayer ion-repulsion potential [64], and the second terms by the Coulomb attraction. For metals, the positive terms in (15) are approximately equal to the sum of the repulsion forces (kinetic, "zero" pressure of the electrons, interaction between the closed shells of the ions, etc.), while the negative terms represent the attraction forces (Coulomb and exchange forces etc.). By specifying particular constants in (15) one can determine the variation of the functions $P_c(v)$ and $E_c(v)$, and then also $\gamma_{eq}(v)$ with the aid of (9). Knowledge of these relations, and also of the thermal electronic components of the pressure and of the energy makes it possible, in turn, to construct the dynamic adiabats.

The real zero isotherms and $\gamma_{eq}(v)$ curves correspond to a combination of constants that approximate in best fashion the experimental data on shock compression. To compare the calculated adiabats with experiment, it is advantageous to use shock adiabats of "continuous" samples, and furthermore in the region where the thermal electronic terms play the role of corrections. In this case errors in the values of the electronic components cannot appreciably distort the results of the analysis. Their proper parameters, as well as the effects of anharmonicity, can in turn be corrected and determined from the upper sections of the adiabats, especially from the shock-compression curves of porous samples, for which thermal pressures and thermal energies are dominating.

The equations of state considered above do not take into account the melting of the substance behind

the front of the shock wave. This question was considered by Urlin and Ivanov [65].

3. DETONATION OF CONDENSED EXPLOSIVES AND SHOCK COMPRESSION OF SUPERDENSE GASES

A detonation wave is a supersonic compression wave, behind the front of which the explosion energy is released. The passage of the detonation wave converts the chemicals in the solid and liquid explosive substances (ES) into mixtures of gaseous explosion products (EP) with density of 2.0 g/cm^3 and higher. This, of course, is accompanied by high temperatures and pressures and by large translational velocity of the explosion products in the direction of motion of the detonation front.

The classical hydrodynamic theory of detonation processes was developed abroad in the 19th and 20th centuries by Chapman [67], Michelson [33], and Jouguet [68]. It was further developed principally by Zel'dovich [59], Neumann [70], Taylor [71], Landau and Stanyukovich [49], and Stanyukovich and Pokrovskiĭ [72,33].

Under stationary conditions the detonation speed is a thermodynamic characteristic of the substance, and does not depend on the initiation conditions. According to the Chapman-Jouguet condition, it is equal to the rate of propagation of the perturbations in the reacting matter behind the front of the wave (D = U + C, C = speed of sound in the explosion products). On a P-v compression diagram (Fig. 12), the detonation speed is determined by the slope of a line tangent to the adiabat of the explosion products, while the state on the front is determined by the coordinates of the tangency point.

We do not have sufficient knowledge of the properties of superdense gases for an unambiguous theoretical determination of the quantitative characteristics of detonation processes in condensed explosives.

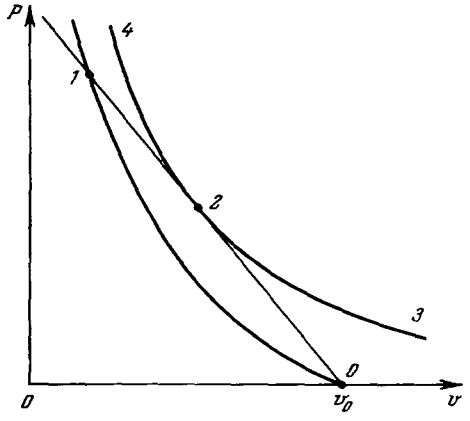

FIG. 12. Shock adiabats of detonation products and of initial explosive substance. 0 – 1 – adiabat of initial explosive; 2 – 3 – 4 adiabat of explosion products; 2 – Chapman-Jouguet state.

In particular, rather contradictory notions prevailed until recently even for such an important explosion characteristic as the pressure at the Jouguet point. Schmidt's theory [73], for example, gave the detonation pressure of trotyl 120 kbar, whereas the Landau-Stanyukovich theory [49] gave 190 kbar.*

The development of dynamic research methods has made it possible to supplement the registration of detonation speeds with direct measurements of the dynamic parameters of the detonation waves. This problem was solved in the late Forties by several different methods.

Sof'ina and Tsukerman determined the detonation parameters from the relative displacements of foils which were located at different distances from the detonation front at the instant of pulsed x-ray photography.

The use of large charges and plane detonation waves has made it possible to avoid in these investigations the influence of the expansion waves, which distort the results of the x-ray investigations made by Schall [21].

In the "partition method," the detonation parameters were determined from the reflection of a plane detonation wave from samples having different dynamic rigidity, i.e., with different values of $\rho_{0M}D_M$ (ρ_{0M} is the initial density of the partition and D_M is the wave velocity in the partition). The first investigations in this direction were made in the USSR by Al'tshuler and Krupnikov in 1948 [36]. As follows from the review [21] and from a 1955 paper [44], an analogous procedure was developed and used by Goranson in the USA in 1945.

In investigations of this type the experimentally measured quantities are the mass and wave velocities in the partitions (see Fig. 5), the product of which, in accordance with (1b), determines also the reflection pressure. The conversion from the states in the partitions to the detonation parameters is based on the equality of the pressures and velocities on both sides of the boundary between the explosive and the partition. On the pressure-velocity diagram (Fig. 13), the lines $P = \rho_{0E}SD$ are the geometric loci of the points corresponding to a specified detonation speed.

In the case of reflection from partitions that have a larger dynamic rigidity than the explosion products ($\rho_{0M}D_M > \rho_{0E}SD$), the explosion products are decelerated and the pressures increase, while in the case of reflection from less rigid partitions we have expansion with reduced pressure.

The states obtained in experiments with different partitions determine in the aggregate the curve AB and the Chapman-Jouguet point where this curve crosses the detonation line.

*Here and throughout the pressure will be given in units of bar = 10^6 dyne/cm^2 = 1.019716 kg/cm^2 = 0.986924 of normal atmosphere; 1 kilobar (kbar) = 10^3 bar, and 1 megabar (Mbar) = 10^6 bar.

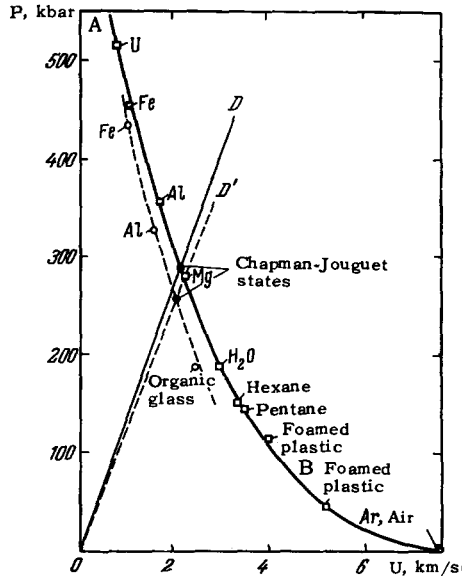

FIG. 13. P-U diagram of reflection of detonation from partitions of different rigidity. – wave line $P = \rho_0 ESDU$ and experimental curve of reflection for alloy B (PG-36/64); – – – the same for the alloy TG-50/50.

Owing to the attenuation of the shock waves, the true states of reflection are found by measuring the mass-velocities at different partition thicknesses and extrapolating the results to the separation boundary. Figure 13 shows the experimental points obtained in this manner and the curves drawn through these points for two alloys of trotyl and hexogen. The lower curve, corresponding to 50% trotyl content (TG-50/50) was obtained by the authors of [36]. The upper curve duplicates the data of Deal [74] (USA), who investigated

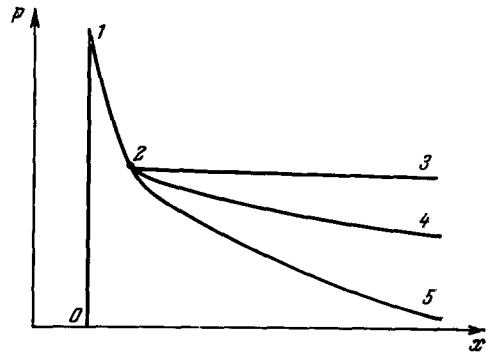

FIG. 14. Profile of detonation wave. 2 – 1) stationary zone of chemical reaction; 2 – 3, 2 – 4, 2 – 5) rarefaction waves along different detonation paths.

alloy "B" (36% trotyl and 64% hexogen).

The Jouguet pressures of these compounds are 260 and 292 kbar, respectively, and the mass velocities are 2.05 and 2.12 km/sec. For trotyl and hexogen, the results of analogous investigations by Deal [75] and Dremin [76,77] are shown in the left part of Table I together with the data on the alloy "B."

The main cause of differences in the values of the parameters obtained in [75-77] is most likely the difficulty of separating the gasdynamic parameters of the Jouguet state from the increased pressures of the reaction zone. The same point of view is adhered to in [78] by Dremin et al. The existence of a "chemical peak" of pressures was predicted theoretically by Zel'dovich [69] and by Neumann [70].

According to [69,70], the zone of chemical decomposition, which carries the peak of pressure P_1 (Fig. 14), forms the leading front of the wave and moves through the charge at the detonation speed.

Table I. Experimental and calculated [58] parameters of detonation waves

Explosive	Author	Deal[75]	Dremin[76,77]	Zubarev[58] (calculation)	P_T/P, % [58]
TNT, $\varrho_0 = 1.637$ g/cm³	D, km/sec	6.942	7.09	7.04	
	U, km/sec	1.664	1.87	1.60	48
	P, kbar	189.0	217.0	184.0	
Hexogen, $\varrho_0 = 1.767$ g/cm³	D, km/sec	8.639	8.70	8.88	
	U, km/sec	2.213	2.42	2.08	34
	P, kbar	338.0	372.0	327.0	
Composition "B" (TNT/hexogen 36/64) $\varrho_0 = 1.713$	D, km/sec	8.018	7.96 *)	—	
	U, km/sec	2.127	2.18 *)		40
	P, kbar	292.0	298.0 *)	—	

*Obtained by interpolation[76].

The minimum pressures P_1 of the front are determined by the intersection of the detonation line 0—1 with the adiabat of the undetonated explosive (see Fig. 12). On the other limit of the zone are realized states 2 of Chapman-Jouguet.

The motion of the explosion products is described by self-similar isentropic expansion waves. To the contrary, the reaction zone is stationary: the pressure and velocity distributions in it do not depend on the detonation path (see Fig. 14).

By carefully measuring the initial velocities of motion of thin plates, Duff and Houston [79], and later Dremin and Pokhil [80] succeeded in detecting a region of increased pressures characteristic of the first stage of motions of the shock waves in partitions. Their results for two condensed explosive substances—trotyl and alloy "B"—are shown in Fig. 15. The ordinates are the initial velocities of aluminum partitions, and the abscissas their thicknesses. The curve for trotyl contains also points registered with a polaroid pressure pickup by Eichelberger and Hauver [81], and on the curve for alloy "B" are points obtained by Deal [75] for charges whose lengths exceeded by a factor of 3 the lengths of the charges used in the experiments of Duff and Houston.

The dimensions of the stationary zone can be determined experimentally by comparing the attenuation curves obtained for charges of different length. Such comparisons have not yet been made on an exhaustive scale. For alloys of trotyl and hexogen and for other brisant explosives, the stationary section of the attenuation curve certainly does not exceed several millimeters, as would follow in particular from Fig. 15. Duff and Houston assumed a value of 1 mm

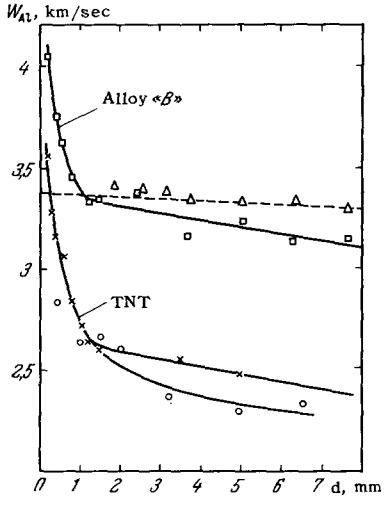

FIG. 15. Curves showing attenuation of shock waves in aluminum partitions. □, △ – data of Duff and Houston[79] and Deal [75] for alloy "B" reduced to the density $\rho_0 = 1.713$ g/cm³. Charge lengths 70 and 200 mm; ×, ○ – data of Dremin and Pokhil[80] and Eichelberger and Hauver[81] for TNT. The high velocities of motion of the thin partitions characterize the increased pressures of the chemical zone.

for the alloy "B", identifying the Jouguet state with the point of inflection of the W(d) curve. In this case the time of existence of the increased pressures is equal to 0.02 μsec, and the length of the reaction zone in the charge is 0.13 mm.

In his latest paper [78] Dremin proposes, in contrast with [79] and [80], much larger dimensions for the reaction zones, by a factor 5—10.

These notions contradict the stationarity condition. The degree to which this condition is indispensable should be established by a more highly perfected and more accurate theory of the question, based on a simultaneous solution of the nonstationary problems of hydrodynamics and the equations of chemical kinetics. It should also take into account the inhomogeneities of motion in the case of detonation of the spin type, which according to [82] can occur in condensed explosives. (This question is debatable; the results obtained in [82] are disputed in [83].)

A very effective method of investigating detonation processes is the magneto-electric method of recording mass velocities, proposed in 1948 by E. K. Zavoĭskiĭ.

To carry out experiments by this method, a thin U-shaped aluminum pickup is imbedded in a charge placed in a homogeneous magnetic field (Fig. 16). The speed of the explosion products is determined from the emf produced when the pickup cuts the magnetic flux lines.

Zaĭtsev, Shvedov, and Pokhil [84] and Dremin and Shvedov [78] used the magneto-electric procedure to determine the Jouguet parameters of trotyl, hexogen, their alloys, and some other substances. The data obtained in this manner are close to those obtained with partitions, both in absolute magnitude and in the degree of reproducibility of the results. The same method was used in [78] to detect an increase in velocity in the reaction zone.

The magneto-electric method makes it possible to observe the velocity of the explosion products during prolonged time intervals, i.e., to determine the pro-

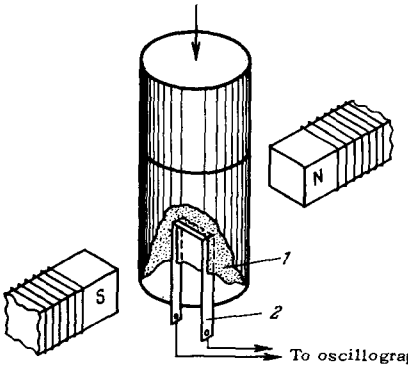

FIG. 16. Diagram of magneto-electric method of Zavoiskii for the measurement of velocity of explosion products. 1 – Explosive charge; 2 – U-shaped pickup of aluminum; N, S – poles of electromagnet.

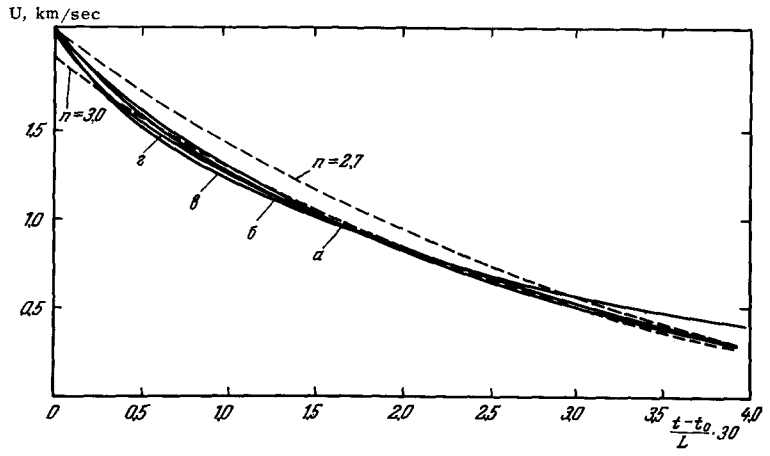

FIG. 17. Form of self-similar expansion wave explosion products for the alloy TG-50/50[86]. $[(t-t_0)/L] \times 30$ – dimensionless time. a) Experimental curve for a charge of L = 5 mm; b) L = 15 mm; c) L = 30 mm; d) L = 60 mm. The theoretical curves for the explosion-product equations of state $P = Av^n$ are shown dashed.

file of a detonation wave. For the TG-50/50 alloy, velocity distribution curves were obtained by Zubarev [86] for charges from 60 to 5 mm in length. After eliminating a small stationary interval $\tau = 0.1$ μsec (this interval includes the apparatus constant in addition to the reaction time), it became possible to represent the results obtained with different charges in dimensionless form by a single dependence describing a self-similar expansion wave (Fig 17). The dashed curves in the diagram show the wave profile corresponding to the simplest expansion law $P = Av^{-n}$ with n = 2.70 and 3. Actually, according to [86], the isentropic exponent is a variable quantity.

Definite progress was made towards clarification of the nature of the repulsion forces responsible for the appearance of high explosion pressures. Until recently it was unclear to what extent their origin lies in the thermal motion of the molecules of the heated explosion products, or in the elastic deformation of the molecules.

To answer this question and to construct the equations of state of explosives, Zubarev and Telegin [56] undertook investigations of two components of the explosion products—carbon dioxide and nitrogen. Even earlier, foreign and Soviet authors investigated the shock-compression curves and the equation of state of water [87-89] and graphite [90].

The experiments described in [56] were made in dry ice and liquid nitrogen, and covered the pressure range from 20 to 700 kbar. The results obtained are plotted in pressure-density coordinates in Fig. 18, together with the shock adiabat of water. On the basis of the shock-compression curves, the authors of [56] derived consistently the equations of state of the individual components, and then the equations of state of their mixture that forms the explosion products [57,58].

To derive the equation of the components from the experimental data, constants were chosen for the molecule interaction potential. The thermal properties were described by the "free volume" theory. Their relative amounts in the explosion products were determined from the conditions of chemical equilibrium.

The theoretical accuracy attained in [58] is demonstrated by comparison of the calculated and experimental detonation speeds (Fig. 19).

As follows from the curves and from Table I, the difference between theory and experiment does not exceed 3%. Greater discrepancies are possible in the pressure calculations. The Jouguet state (Fig. 12) is the place where the line $P = (v_0 - v)D^2/v_0^2$ is tangent to the adiabat of the explosion product. The position of the point of tangency depends strongly on small changes in the configuration of the adiabat, and consequently on the small inaccuracies in the equation of state of the explosion products.

Calculations made in [58] yielded the relation between the thermal and "cold" pressures. The total pressure of the detonation waves is approximately 35–45% thermal and 65–55% the result of the elastic

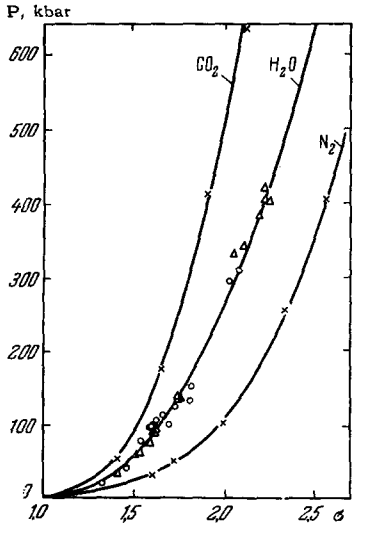

FIG. 18. Dynamic adiabats of carbon dioxide[56], nitrogen[56], and water[87,89]. Experimental points: △ – from [87]; ○ – from[89].

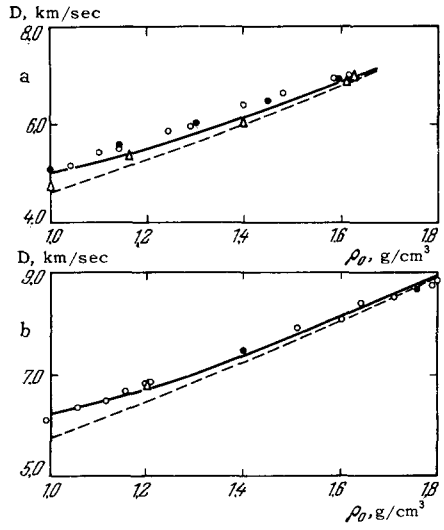

FIG. 19. Experimental and calculated relations for a) trotyl and b) hexogen (after[58]). – – – constant composition of explosion products, corresponding to minimum volume, —— – variable composition of explosion products, calculated from the conditions of chemical equilibrium.

reaction of the explosive molecules to the compression.

Of great significance for the construction and verification of the equations of state of explosive products would be a determination of the detonation temperatures. In this field there are so far very few investigations[23,26], the results of which are not in agreement.

More direct are the measurements of Voskoboĭnikov[26] on transparent and semitransparent substances. However, even under these conditions the interpretation of the experimental data is made difficult by the complex structure of the detonation front and by the uneven distribution of the temperatures over its width.

An extensive set of investigations is devoted to the onset and development of detonation waves under the influence of shock pulses of different intensity. A sufficiently complete review of these investigations is given in [21], in the proceedings of the 1961 Paris Conference devoted to questions of detonation [98], and in [91].

4. SHOCK ADIABATS AND ZERO ISOTHERMS OF METALS

The most extensive application of the dynamic methods was for the study of metals. The first papers of Goranson et al.[44], Walsh and Christian,[47], and Mallory [45], devoted to shock compression of aluminum, copper, lead, iron, and cadmium at pressures up to 500 kbar, were published in 1955. In 1957 were published the extensive researches of Walsh et al.[92] on shock compression of 27 metals and their equations of state for the same range of pressures. The results of Al'tshuler, Krupnikov, Ledenev, Brazhnik, and Zhuchikhin, who extended the experimentally investigated region of pressures in 8 metals by a factor 10, i.e., to 5 Mbar, were published in the following year.

In the main, these investigations were performed in 1948–1950. In the years that followed, Krupnikov, Bakanova, Trunin, and Al'tshuler extended the range of pressures even further, to 9–10 Mbar[42,43], and checked and refined the earlier results.

In 1960–1962, the pressure ceiling was raised by McQueen and Marsh[40] (USA) to 1.6–1.8 Mbar and by Morris and Skidmore[41] (England) to 6.5 Mbar. The highest degrees of compression of metals, by a factor 2.7–3.4, were obtained by Bakanova, Trunin, and Dudoladov [93] in investigations of alkali metals. High pressures were produced in all cases by using the investigated samples to stop strikers accelerated by explosion products to very high velocities, 5–14 km/sec. The general status of experimental research on shock compressibility of metals is illustrated by the pressure-density diagram on Fig. 20, which shows 23 shock adiabats. The adiabats of 9 metals, known up to pressures of 0.5 Mbar, as

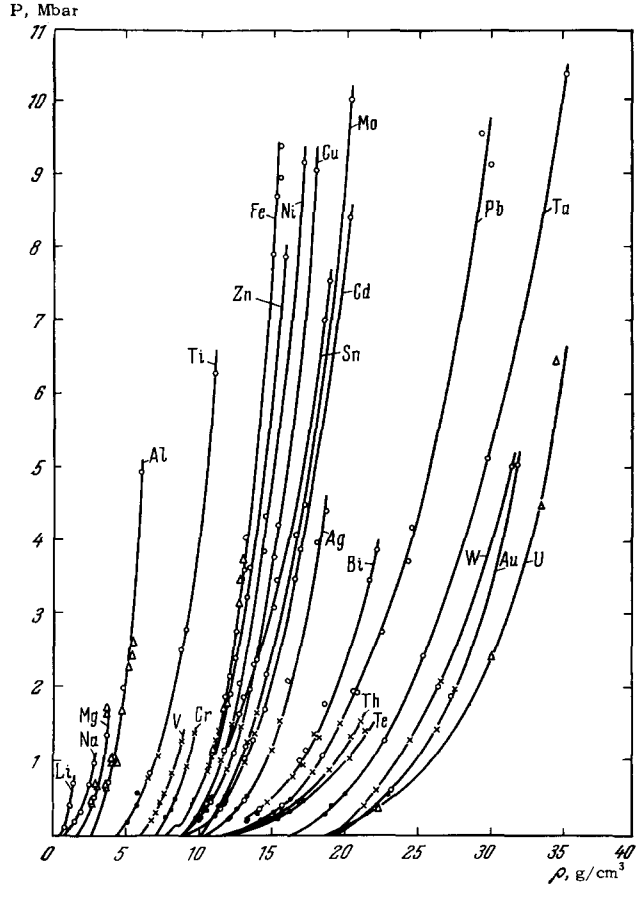

FIG. 20. Shock adiabats of 23 metals. ●– data of Walsh et al et al[92] (USA); × – McQueen and Marsh (USA)[40]; ○ – Soviet investigators[36,39,38,42,43,93,54]; △ – experimental points of Skidmore and Morris[41] (England).

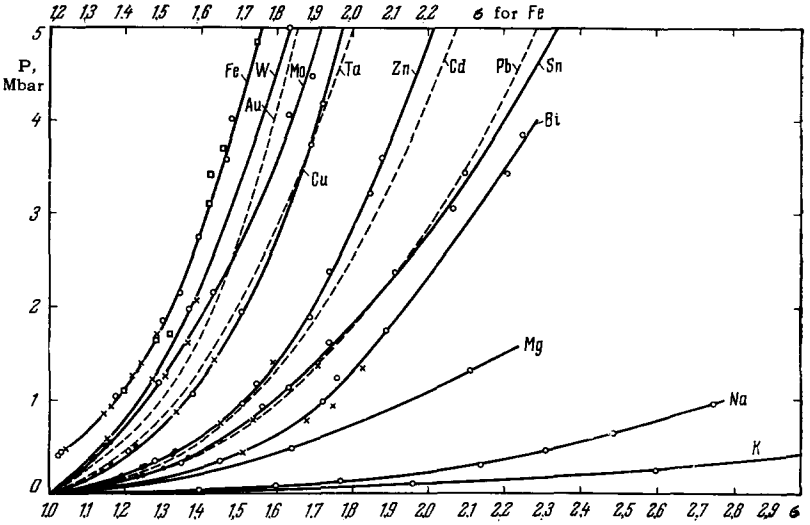

FIG. 21. Shock compression curves of 32 metals as functions of their relative density $\sigma = \rho/\rho_0 = v_0/v$. × – data of McQueen and Marsh[40]; o – experimental points obtained in the Soviet Union[36,38,39,42,43,93]; □ – data of Skidmore and Morris[41].

well as the adiabat of cobalt, which in accordance with [40] overlaps the adiabat of copper, are not shown in the figure. The results of Walsh et al.[92] predominate at the 500 kbar level and those of Soviet researchers prevail at pressures above 2 Mbar [36,38, 39,42,43,54,93].

The differences in the compressibilities of metals are very clearly evidenced on the plot of pressure against relative density (Fig. 21).

The most compressible are alkali and alkali-earth metals, and among the elements with larger atomic numbers—lead, tin, and bismuth. The greatest rigidity is possessed by transition metals with large d-electron covalent bond—tungsten, tantalum and molybdenum. Copper and gold show a similar behavior. Zinc and cadmium occupy an intermediate position.

A striking feature is the good agreement of results obtained independently in the Soviet Union, USA, and England for iron.

By way of an example, Table II gives in greater detail data obtained in [42] with samples of copper and cadmium, at different iron striker speeds W_S. The densities of the samples were more than doubled by the high pressures. The increase in the wave velocities is quantitatively characterized by the sharp increase in the average modulus of shock compression $\rho_0 D^2 = Pv_0/(v_0 - v)$: at the largest impact speeds, the per-unit internal energies of the investigated material are very large. For cadmium and copper they exceed by 6—7 times the energy of explosion of trotyl. Expansion from these states is accompanied by explosion and atomization of the metals. Even greater concentrations of thermal energy were attained by shock compression of metals with lower density, with initial per unit volume $v_{00} = mv_0$.

The first experiments on the compression of porous iron are described in [36]. The first large scale experimental investigation in this direction was made by Krupnikov, Brazhnik, and Krupnikova[94], who recorded shock adiabats of powdered tungsten with porosities m = 1.8, 2.2, 3.0, and 4.0 (Fig. 22).

The experiments have confirmed the paradoxical deduction of the theory, namely that application of shock pressures of several megabars to powders of low density can not compress them even to the normal density of metallic tungsten. This is prevented by the thermal pressure of the atoms and electrons. Up to pressures of 1 Mbar, the configuration of the tungsten adiabats corresponds approximately to the scheme of Fig. 4 with constant value h = 2.10 (γ = 1.82). At larger pressures the upper branches of the adiabats swing sharply to the right, thus evidencing an increase in the effective value of h (a decrease in γ).

Two principal causes lead to a decrease in the

Table II. Parameters of shock compression of copper and cadmium by strong shock waves

Copper						Cadmium				
W_y, km/sec	D, km/sec	U, km/sec	σ	P, Mbar	$E \cdot 10^{-3}$, J/g	D, km/sec	U, km/sec	σ	P, Mbar	$E \cdot 10^{-3}$, J/g
5.60	8.06	2.71	1.506	1.95	3.67	7.16	2.88	1.604	1.79	4.15
9.10	10.58	4.43	1.720	4.19	9.80	9.55	4.67	1.958	3.85	10.90
14.68	14.20	7.15	2.014	9.07	25.60	12.99	7.49	2.362	8.41	28.08

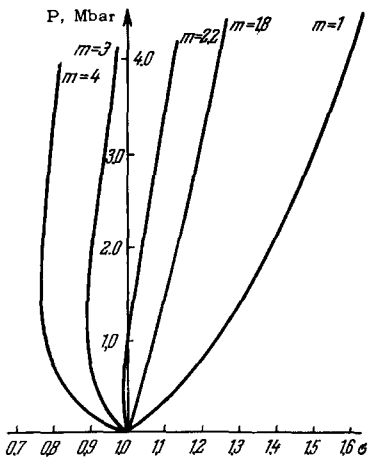

FIG. 22. Experimental shock adiabats of tungsten of different porosity, after Krupnikov[94].

mean value of γ: an increase of the relative role of the electrons with values $\gamma_e < \gamma_{eq}$, occurring during the heating, and a decrease of the value of γ_{eq} with increasing temperature.

The pioneer work of Krupnikov was further developed by Kormer, Funtikov, and others [54], who performed similar experiments in a larger pressure range and on a larger number of metals, of both the transition type (Ni) and simple ones (Al, Cu, Pb). The adiabats obtained in [54] for copper and nickel with porosity m = 3 are shown in Fig. 23.

Using the high sensitivity of the "porous" adiabats to changes in the thermodynamic characteristics of metals, Kormer and his co-workers succeeded in recording and differentiating the influence of the anharmonicity of the oscillations of the atoms from the excitation of the electrons and, as shown in Fig. 23, observed a difference in the behavior of simple and transition metals. The greatest energy concentrations attained upon compression of highly porous

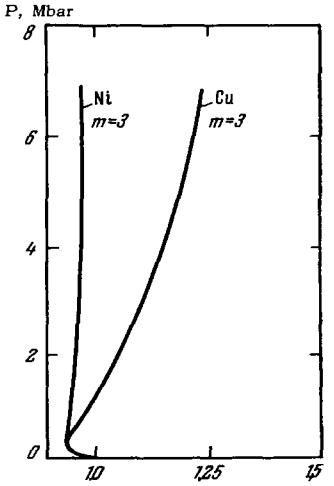

FIG. 23. Shock adiabats of porous nickel and porous copper after Kormer and Funtikov[54].

copper (m = 4) amounted to 60×10^3 J/g in [54], which is 15 times larger than the explosion energy of trotyl.

Let us discuss in greater detail the thermodynamic characteristics of the electron gas, knowledge of which is essential for the construction of the equations of state of metals. Unlike dielectrics, the free energy levels in metals are directly adjacent to the Fermi surface, which bounds in momentum space the energy states occupied by the electrons.

When the metal is heated to a temperature T, the number of excited electrons is proportional to the number of levels νkT (ν—level density, k—Boltzmann constant) at the depth of the energy interval kT. Inasmuch as the average energy acquired by each of the electrons is $\sim kT$, the total thermal energy of the excited electrons is $\sim \nu T^2$. We write it down, as usual, in the form $E_{t.e} = \beta T^2/2$, noting that β is a factor proportional to ν, and consequently dependent on the volume. On the basis of the thermodynamic equation

$$P = T \int_0^T \left(\frac{dE}{dv}\right)_T \frac{dT}{T^2}, \qquad P_{t.e.} = \frac{\gamma_e}{v}\beta T^2$$

with

$$\gamma_e = \frac{d \ln \nu}{d \ln v} = \frac{d \ln \beta}{d \ln v}.$$

The coefficient γ_e is the analog of the Gruneisen coefficient for the lattice. This parameter was introduced into the empirical equations of state of metals by Kormer [39,60], and Zharkov [62]. To describe the thermal properties of the electron gas, Kormer made a detailed analysis of the temperature behavior of electrons, on the basis of the quantum-statistical calculations of Gilvary [95,96] and Latter [97].

This analysis has shown that up to temperatures of the order of 30,000—50,000°, the specific heat of the electrons, as in the model of free electrons, is proportional to the temperature: $C_{t.e} \sim T$, $E_{t.e} \sim T^2$. As to the thermal pressure, the statistical values of γ_e in the experimental range of compressions are to a high degree of accuracy constant and equal to $\frac{1}{2}$. For a free electron gas $\gamma_e = \frac{2}{3}$.

The equation of state (13) obtained in [39] on the basis of statistical considerations is given in Sec. 2.

The experimental values of the molar specific heats $A\beta$ and the coefficients γ_e for several simple and transition metals are listed in Table III. They were obtained [34,98,99] by measuring the specific heats and the coefficients of linear expansion under normal densities and temperatures close to 0° K. As shown by experiment, the level density depends strongly on the band structure of the metals. For simple metals, the electronic specific heats are in crude agreement with the values calculated for bound electrons by means of the Thomas-Fermi statistical theory of the atom.

In transition metals with unfilled d-bands these specific heats are, as a rule, one order of magnitude

Table III. Coefficients of electronic specific heat and coefficients γ_e for simple and transition metals; the γ_e^* were obtained in dynamic experiments

Metals	Al	Cu	Pb	Fe	Cr	Ni	W
$A\beta$, J·mole^{-1}deg^{-2}·10^4	14.5	7.4	31	50	16	73	14.5
γ_e [98, 99]	2.0	0.7	0.8	2.2	—8.0		0.2
γ_e^* [55, 42]	0.5	0.5	0.8	1.5	2.2	1.0	

larger than for simple metals. Even more dependent on the concrete structure of the energy bands and on the character of their crossing of the Fermi surface are the coefficients γ_e.

As follows from Table III, these coefficients can assume a great variety of values, both positive and negative, thus pointing to the existence of negative electronic components of the thermal pressure. The latter takes place in all cases when the compression leads to an increase in the densities of the levels at the Fermi surface, for example, when it approaches the band boundaries or in the case when it comes very close to the lower edge of the d-band.

The anomalies of thermodynamic quantities can occur, according to Lifshitz [100], also when separated regions of the Fermi surface are produced, and under other violations of its topological structure.

The quantities in the third line of Table III were obtained, as already mentioned, at low temperatures. In momentum space they characterize the structure of the bands in a narrow layer adjacent to the Fermi surface. Experiments [54] with porous metals have made it possible to fix the values of the coefficients γ_e at high temperatures, leading to a repopulation of the electrons over the levels of a broad energy band. Together with the data on iron from [42] and chromium, the values of γ_e for Al, Cu, Ni, and Pb are listed in the lowest line of Table III. For simple metals they are close to the quantum-statistical value $\gamma_e = \frac{1}{2}$. For transition metals, the high-temperature γ_e are approximately 2 or 3 times larger.

The compression and heating of metals make the electron distribution in the atom closer to the quantum-statistical distribution. As a result, the statistical treatment of the thermal properties of the electrons, given by (13), is valid at least for simple metals. It is undoubtedly oversimplified for the transition metals. The use for such metals of equations of state similar to (13) with different values of γ_e, exceeding $\frac{1}{2}$ [62,54,42,43] or dependent on the volume, does not solve the problem, since the high-temperature electronic specific heats of these metals are still unknown at present.

Following the concepts developed in Sec. 2 and in the present section, the authors of [39,42,43,54,93] obtained semi-empirical equations of state and the zero isotherms for aluminum, copper, lead, cadmium, tin, zinc, and three alkaline metals, and with lower accuracy for iron, nickel, tantalum, titanium, and molybdenum.

The question of the equation of state of iron was considered from a somewhat different point of view by Zharkov [62] and in [36], where the generalized coefficient γ was obtained from experimental data.

For a smaller range of pressures, 500 kbar and 2 Mbar, the simplified equations of state of Mie-Gruneisen were obtained for a large number of metals by Walsh, Rice, and others [92,28] and by McQueen and Marsh [40]. By way of an example, the relative positions of the dynamic adiabats and zero isotherms, as obtained in [42,40,60] for copper and lead, are shown in Fig. 24.

The main characteristics of the shock-compression process in lead, in accordance with [42], are listed in Table IV. At 9 Mbar, as shown in Fig. 24 and in

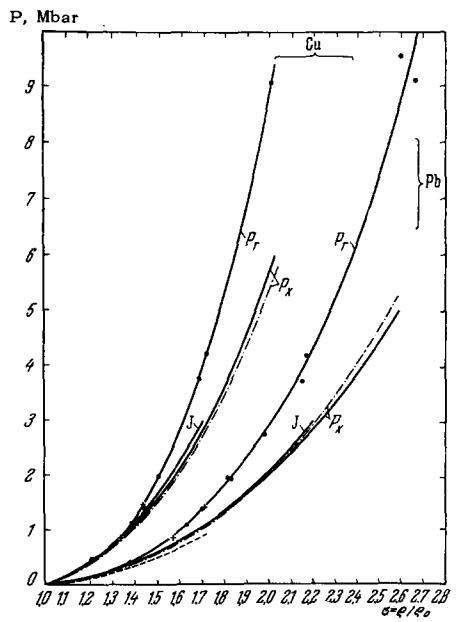

FIG. 24. Shock adiabats (P_H) and zero isotherms (P_c) of lead and copper. J(σ) – zero isotherms in the "sonic" approximation[37] (see Sec. 5): – – adiabats and zero isotherms[42]; – – – zero isotherm of lead[40]; –·– –zero isotherms[60].

Table IV. Characteristics of shock compression of lead [42] ($P_{t.l}$ and $E_{t.l}$—thermal pressure and thermal energy of lattice, $P_{t.e}$ and $E_{t.e}$—thermal pressure and thermal energy of electrons)

σ	P_H, Mbar	P_c, Mbar	$P_{t.l.}$, Mbar	P_{Te}, Mbar	$E_H \cdot 10^{-3}$, J/g	$E_e \cdot 10^{-3}$, J/g	$E_{t.l.} \cdot 10^{-3}$, J/g	$E_{Te} \cdot 10^{-3}$, J/g	$T \cdot 10^{-3}$, °K
1.4	0.46	0.40	0.06	0.00	0.61	0.36	0.22	0.03	2.10 (2.00)
1.6	0.97	0.78	0.17	0.02	1.63	0.80	0.64	0.19	5.70 (8.30)
1.8	1.76	1.32	0.37	0.07	3.48	1.45	1.31	0.72	11.60
2.0	2.84	1.99	0.64	0.21	6.29	2.25	2.18	1.86	19.10
2.2	4.32	2.81	1.00	0.49	10.42	3.21	3.25	3.95	28.50
2.4	6.30	3.84	1.46	1.00	16.25	4.38	4.52	7.35	39.80
2.6	8.88	5.00	2.03	1.85	24.13	5.52	6.02	12.6	53.00

Table IV, the total pressure is 44% thermal, and the total energy is 77%. The contribution of the electrons to the thermal pressure and to the thermal energy is in this case 48 and 68%, respectively.

A noticeable influence of thermal excitation of the electrons on the shape of the shock adiabat appears at 4 Mbar and at the temperature of shock compression even at 1 Mbar. This is evidenced by a comparison with the results of Marsh and McQueen [40] (given in the parentheses), who confined themselves in their analysis to the lattice terms only.

In Fig. 25, the zero isotherms $P_c(v)$ and the shock adiabats of copper and lead were extrapolated [42] to pressures of hundreds and thousands of megabars. With increasing pressure, the disparity between the $P_c(v)$ and $P_H(v)$ curves increases progressively. Whereas the dynamic adiabats tend to a finite value of the limiting density, the increase in density under isothermal compression proceeds without limit. Knowledge of the course of the zero isotherms of many elements makes it possible to trace the transformations of the atomic-volume curves.

Figure 26 shows a plot of v(Z) for elements with small and medium Z at four different pressures 0 and 100 kbar, and 1 and 10 Mbar.

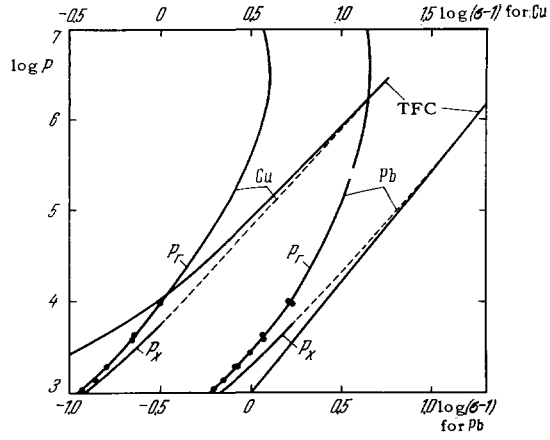

FIG. 25. Extrapolation of shock adiabats (P_H) and zero isotherms [42] (P_c) of lead and copper (P is in kbar). 1 TFC—Calculated zero isotherms after Kalitkin [3]; – – – extrapolated sections of zero isotherms.

At 10 Mbar, the periodicity of the volumes, reflecting the shell structure of the atoms, is already quite weakly pronounced. At still higher pressures (100 Mbar), the v(Z) curve is described by a monotonic almost-linear dependence.

5. SPEED OF SOUND AND ISENTROPIC ELASTICITY OF SHOCK-COMPRESSED BODIES

The speed C of propagation of small sonic perturbations behind the front of shock waves is determined by the isentropic compressibility of the sub-

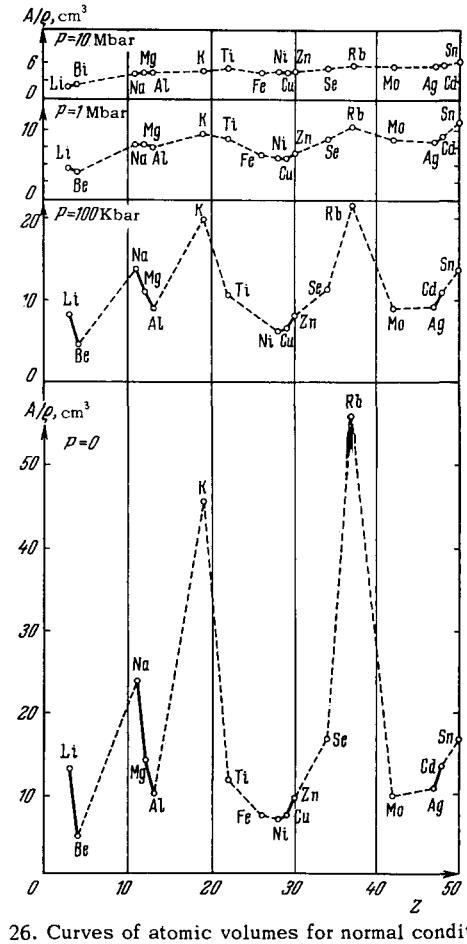

FIG. 26. Curves of atomic volumes for normal conditions at pressures 0 and 100 kbar and 1 and 10 Mbar.

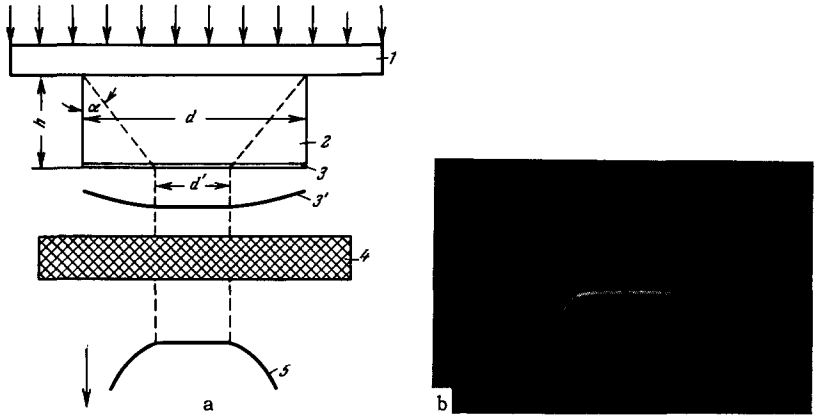

FIG. 27. Determination of the speed of sound by the "lateral relaxation" method[37]. a) Diagram of experiment: 1 – screen; 2 – sample; 3 – thin layer of light substance flying away from the surface of the investigated sample; 3′ – the same layer in flight; 4 – organic glass partition; 5 – scheme of photochronogram, registering the difference in time that the layer strikes the partition. b) Reproduction of photochronogram taken with a slit photochronograph.

stance, and can serve in turn for the calculation of the slope of the isentropes.

$$\left(\frac{\partial P}{\partial \varrho}\right)_S = C^2$$

and of the modulus of isentropic elasticity $K_S = \rho(C^2)$ at high pressures.

Special interest attaches to the measurement of the speed of sound in geophysics, for a more complete interpretation of seismic data. Knowledge of the speed of sound is also necessary for correct planning of dynamic experiments under conditions in which the influence of the relaxation waves must be excluded. At the same time, the greatest significance of these researches, as will be shown presently, is for the study of the equations of state, as an independent method of experimentally approximating the zero isotherms.

Methods of recording the speed of sound behind the fronts of powerful shock waves were developed during the period from 1948 through 1958 by Al'tshuler, Kormer, Funtikov, Speranskaya, Brazhnik, and Vladimirov. They are described in [37] together with the results of measurements of isentropic compressibility by several methods.

The existence of relaxation waves is easiest to detect when a shock wave passes through a cylindrical sample of steplike form (Fig. 27a). The relaxation source can be the generatrix of the cylinder. At the instant when the shock wave emerges to the end face of the sample, the expansion waves subtend on it a peripheral zone of width $S = h \tan\alpha$. From an easily derived relation we get for the speed of sound

$$C = D\sqrt{\tan^2\alpha + \left(\frac{D-U}{D}\right)^2}.$$

The unrelaxed diameter d′ of the sample, and consequently also $S = (d - d')/2$, are obtained from the change in the velocity of its free surface—under the experimental conditions of Fig. 27a—using the difference in time of impact of an outgoing thin layer, deposited on the sample before the experiment, against a transparent partition. A time-difference curve recorded with a photochronograph is shown in Fig. 27b.

This method was used by the authors of [37] to observe a second system of relaxation waves, moving with speeds much larger than the gasdynamic values of the speed of sound. They were interpreted in [37] as being waves characterizing the elastic stage of expansion of compressed matter. This question will be considered in greater detail in Sec. 11.

More widely used is a second method, based on registration of the attenuation of shock waves produced in a target by impact against a thin plate. The initial scheme of the method was proposed by Zababakhin. A modified variant, together with the results of measurements, are described in [37]. This method was described almost simultaneously and independently by Fowles [101]. The errors connected with the strength effects were considered in [102] and [103].

Figure 28 shows a distance-time diagram of the motion of shock waves and relaxation waves when plates made of identical materials collide. The diagram is given in the hydrostatic approximation, i.e., without account of the strength waves which move with larger velocity. The centered relaxation wave is produced in the form of a diverging set of characteristics at the instant when the deceleration shock wave emerges to the rear surface of the flying plate.

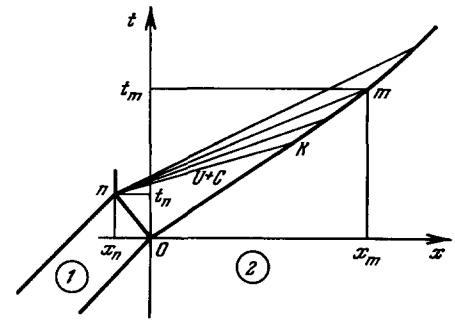

FIG. 28. x-t diagram of the impact of a thin plate (1) against a target (2). Okm – trajectory of shock wave in the target; n – pole of centered relaxation wave; k – start of attenuation.

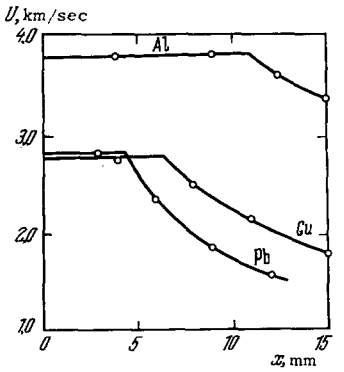

FIG. 29. Curves showing the attenuation of shock waves in targets made of aluminum, copper, and lead[37]. The waves were produced by the impact of a thin 1.5 mm disc, flying with a speed 5.71 km/sec.

The leading front of the relaxation wave moves through the striker and the target with a speed exceeding that of the shock front. The attenuation of the shock wave begins at the overtaking point K.

By recording at an arbitrary point m in the attenuation region the coordinates t_m and x_m of the shock wave, and also the mass velocity U_m, it is possible to find the slope of the m-characteristic $\alpha_m = (x_m - x_n)/(t_m - t_n)$ and the speed of sound $C_m = \alpha_n - U_m$. The organization and interpretation of the experiments remain in principle the same as when different materials are made to collide.

The experimental curves of shock-wave attenuation of shock waves [37] moving through the target are shown in Fig. 29. The striker used in these experiments was a 1.5 mm plate of iron, moving with a velocity 5.71 km/sec. The speed of sound behind the shock-wave front in copper, lead, aluminum, and iron up to pressures of several megabars was determined in [37]. The isentropic moduli

$$K_S = \varrho C^2 = \frac{dP}{d\ln\varrho}$$

for three metals are shown in Fig. 30. In shock compression by a factor 1.70, the elasticity of the copper increases by a factor 7.4, that of iron by 8.6 times, that of aluminum by 10 times, and that of lead by 10.8 times.

The passage of shock waves is connected with irreversible heating of the medium and with an increase in its entropy. Consequently, the shock adiabat is steeper than the isentropes everywhere, except at the origin, and crosses these curves at acute angles.

The upper limit of the possible positions of the zero isotherm is obtained by unifying segments of isentropes into a single curve:

$$J(\varrho) = \int_{\rho_0}^{\rho} \left(\frac{\partial P}{\partial \varrho}\right)_{S_H} d\varrho = \int_{\rho_0}^{\rho} C_H^2 d\varrho. \qquad (16)$$

The subscript H denotes here and throughout that the isentropic derivatives and speeds of sound were determined for the states of the shock adiabats. Inasmuch as the heating at constant volume leads with rare exception, to an increase in elasticity, we have

$$C_H^2 = \left(\frac{\partial P}{\partial \varrho}\right)_{S_H} > \left(\frac{\partial P}{\partial \varrho}\right)_{S=0} = \frac{dP_c}{d\varrho}$$

and consequently $J(\rho) > P_C(\rho)$.

The relative positions of the curves P_H, J, and P_C are shown schematically in Fig. 31.

The function J makes it possible to calculate also the lower limit of the increase in thermal energy

$$\Delta E_{T\min} = \frac{1}{2} P_H(v_0 - v) - \int_v^{v_0} J(v)\,dv < \Delta E_T. \qquad (17)$$

The positions of the curves $J(\sigma)$ of [37] relative to the dynamic adiabats and zero isotherms of copper and lead obtained by another method (see Secs. 2 and 4) are shown in Fig. 24. It follows from the diagram that the representation of the zero isotherms by the functions (16) is in itself a fair approximation. On the other hand, we can now conclude that the "cold"

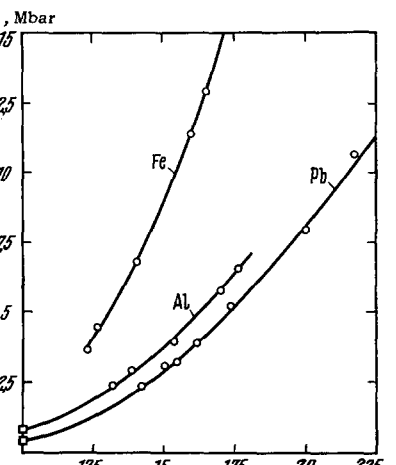

FIG. 30. Dependence of the isentropic modulus K_S of iron, aluminum, and lead on the degree of shock compression[37].

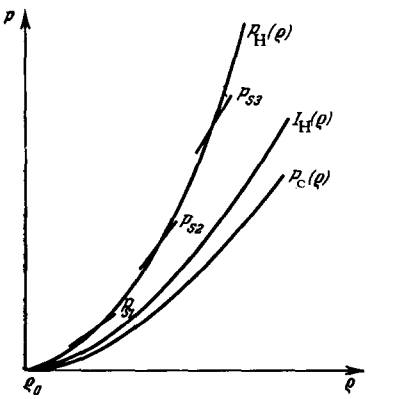

FIG. 31. Relative positions of the shock adiabat P_H, the isentropes P_S, the zero isotherm P_C, and the function

$$J(\varrho) = \int_{\rho_0}^{\rho} C_H^2 d\varrho.$$

pressures, obtained by the methods of Sec. 2, are not overestimates.

A more exact knowledge of the functions J(v) makes it possible to estimate the thermal energies of a compressed body with the aid of inequality (17). According to the data of [37], for strong shock waves the error does not exceed several per cent. If the specific heats are known, the temperatures will be determined with the same accuracy.

The question of the isentropic compressibility behind the front of strong shock waves has so far attracted a limited number of researches. It is to be expected that work in this direction will develop further.

6. COLLISION OF SHOCK WAVES

Processes of frontal and oblique collision of incident shock waves leads to the formation of two new reflection waves, which limit at each given instant of time the deceleration region contained between them.

The degree of increase in pressure upon collision depends on the properties of the medium and on the intensities of the colliding waves. For weak acoustic pulses and frontal collision, the pressure is doubled. With increasing amplitude of the shock waves, the factor by which the pressures are increased also increases. During the course of collision each particle of the matter is compressed twice, —to a pressure P_1 when the incident wave passes (Fig. 32), and then, upon passage of the reflected wave, to a pressure

$$P_2 = P_1 + \frac{D_{12}\Delta U_{12}}{v_1}; \qquad (18)$$

The specific volume decreases in this case to

$$v_2 = v_1 \frac{D_{21} - \Delta U_{21}}{D_{21}}. \qquad (18a)$$

In Eqs. (18) and (18a) the subscript 1 denotes the parameters of the incident waves, ΔU_{21} is the discontinuity in the mass velocities on the front of the reflected wave, and D_{21} its relative velocity. Compared with a single passage 0—3, compression to the same specific volume by successive passages through the states 0—1—2 is accompanied by a smaller increase in the internal energy, by an amount equal to the unshaded area S_{0123}. Consequently, the states produced upon collision lie lower than the single-compression adiabat, and approach the zero isotherm $P_c(v)$. This circumstance explains the possible significance of experiments on double compression for the study of properties of substances and their equations of state at high pressures.

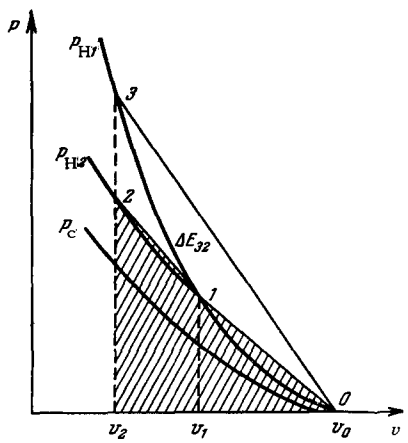

FIG. 32. Comparison P-v diagram of single and multiple compression.

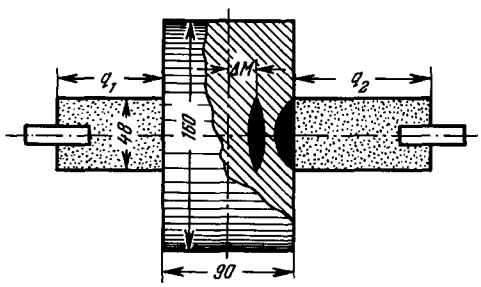

FIG. 33. Diagram of bilateral blast of charges of different size[104].

Interesting pictures of the interaction of colliding shock waves in metals are observed in strong samples subjected to explosive action of several charges. A system of bilateral blast of a cylindrical sample, after [104,105], is shown in Fig. 33.

The dark etched zones on the polished metal surface show the regions of phase transformations induced by pressures of 130 kilobars and more (Section 7). The central lens-like region is the result of superposition of narrow pressure crests, forming the fronts of intersecting waves. The pressure field produced by the interaction of six shock waves, is demonstrated on Fig. 34, which is a reproduction of a photograph from [104] of the etched section of a sample after a six-sided blast. The dark zones stretching along the radii are the results of oblique collision of

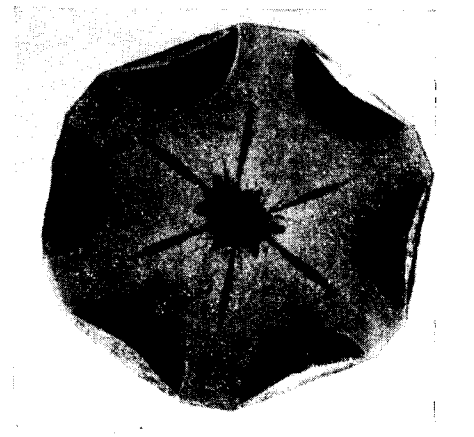

FIG. 34. Macrostructure of metal in the cross section of a steel cylinder when six charges are blasted simultaneously[104].

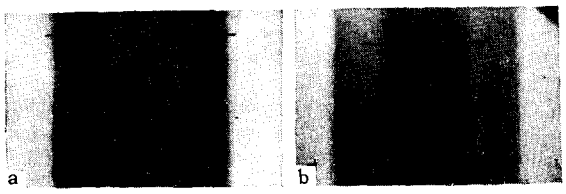

FIG. 35. Compression of paraffin by shock waves colliding head-on. a) Preliminary x-ray picture: L_0 – initial thickness of layer delineated by lead foils; b) explosion x-ray photograph: L – thickness of layer after its compression by the incident and reflected waves.

two neighboring shock waves. The central spot is a result of the superposition of six waves.

A more direct registration of the process of collision of shock waves in paraffin, water, Plexiglas, magnesium, and aluminum was realized by Petrunin and the author in [106], using x-ray photography. The photographs of [106] were obtained with sharp-focus Tsukerman and Manakova x-ray tubes [19], which produced flashes of radiation 0.1—0.3 μsec long. The nominal voltage applied to the tubes was 1.5 MV.

The simplest to interpret are experiments on the frontal collision of two identical waves with flat-top pressure profiles. The x-ray-photograph of Fig. 35a fixes the initial thickness of the layer L_0, separated inside a paraffin block by two thin lead foils. The "blast" photograph of Fig. 35b discloses the layer thickness L_2 after the collision, and the position of the reflected waves.

In this interpretation, the experiments determine the degree of compression $v_0/v_2 = L_0/L_2$, and for known parameters of the incident waves (v_1, P_1, U_1) also the pressure $P_2 = P_1 + U_1^2/(v_1 - v_2)$. In the given case $v_0/v_2 = 2.05$ and $P_2 = 360$ kbar. The main results were obtained in [106] under conditions of inclined collision of shock waves (Fig. 36). The angles of incidence α were set by the experimental conditions, while the reflection angles β were obtained from the pulsed x-ray pictures. The simple relations between these quantities, given in [106], yielded the speed D, the velocity discontinuity ΔU_{12}, and also, through (18), P_2 and v_2. The greatest increase in pressure, by a factor 3.5—4, occurred for the strongly compressible paraffin, Plexiglas, and water,

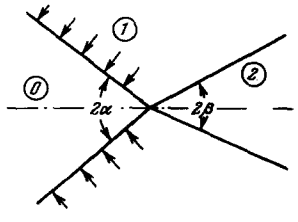

FIG. 36. Oblique collision of shock waves in the regular mode. 0 – region of standstill ahead of the front of the incident wave; 1 – region of single compression behind the front of the incident wave; 2 – region of double compression by the incident and reflected waves.

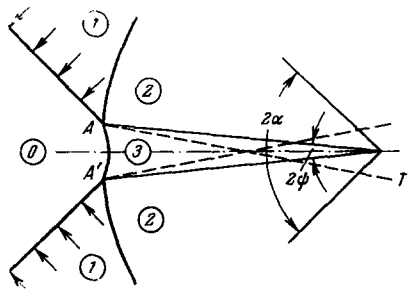

FIG. 37. Diagram of three-shock configuration. Regions 0, 1, and 2 – the same as in Fig. 36. 3 – Region of single compression behind the front of the frontal wave; AA′ – frontal wave; AT – line of tangential discontinuity.

for which an increase in density by 2.2, 2.2, and 2.6 times was attained at 550, 650, and 590 kbar, respectively. The results obtained with magnesium and aluminum were much closer to conditions of collision of acoustic waves.

The pressures behind the reflected waves increase here only by a factor 1.5 under practically indentical angles of incidence and reflection. The described procedure is not universal. Its application is limited to elements and compounds of low atomic weight and collision pressures that are not too high, on the order of 500—800 kbar. The accuracy with which the angles of reflections and the thickness of layers are recorded is likewise not very satisfactory.

Very interesting pictures of a three-shock configuration (Fig. 37) are obtained when shock waves collide at large angles of incidence, exceeding a certain critical value that depends on the thermodynamic properties of the substance. The theory of this phenomenon, discovered in 1878 by E. Mach in a study of air shock waves, was developed in [31]. In solids, the appearance of the frontal wave between two colliding waves was first observed by Feokistova [107] and then subjected to a systematic study by Kormer, Bakanova, and the author [108]. One of the experimental variants realized in [107] and [108] is shown in Fig. 38a. Copies of a photochronogram showing the sequence of emergence of the shock waves on the base of a prismatic sample are shown in Figs. 38b and c. The photochronograms make it possible to determine the velocity of the leading frontal wave, and consequently also the pressure behind its front (for a substance whose shock adiabat is known).

The diagram of Fig. 39 shows the results of the collision pressures registered in [108] for aluminum as a function of the collision angle α. The pressure in the incident wave was 330 kbar. The solid curves on the left part of the diagram describe the regular pre-critical regime. The experimental point given here was obtained in [106] by an x-ray analysis method. Regular reflections are characterized by pressures that are close to one megabar, i.e., the same order as in frontal collisions. The frontal wave,

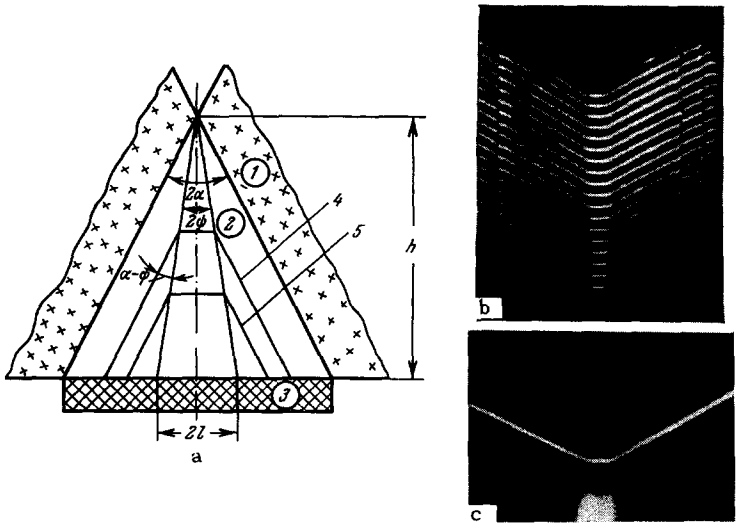

FIG. 38. a) Diagram of experiment on the registration of a three-shock configuration: 1 – charges with plane detonation wave; 2 – prismatic sample with angle 2α at the vertex; 3 – organic-glass plate; 4, 5 – fronts of three-shock configuration at different instants of time; 2ψ – angle at which the frontal wave propagates from the point of its initiation. b) Raster photochronogram of three-shock configuration in aluminum[107]. c) Photochronogram of three-shock configuration in aluminum[108]. The inclined lines of the photograph characterize the speed with which the waves glide over the base of the sample, while the connecting line represents the width of the frontal wave.

as shown by experiment, is produced at an incidence angle 35°. It moves with a velocity of 13 km/sec under the influence of pressures of 2 Mbar, exceeding by a factor of 6 the pressure of the incident waves. With further increase in the collision angles, the amplitudes of the frontal waves decrease rapidly, tending to a value P_1 for glancing motion ($\alpha = 90°$), when the reflected shock waves degenerate into sound waves. Another interpretation of the experiments yielded pressures of 4—7 Mbar in aluminum, iron, and lead for colliding waves with amplitude 1.0—1.8 Mb[108].

According to the universally accepted theory[31], the pressures and the tangential components of the velocities are equal behind the front of the frontal wave in region 3 (see Fig. 37) of single compression, and behind the front of the reflected wave in region 2 of stepwise compression. At the same time, the degrees of compression, and especially the temperatures, are markedly different.

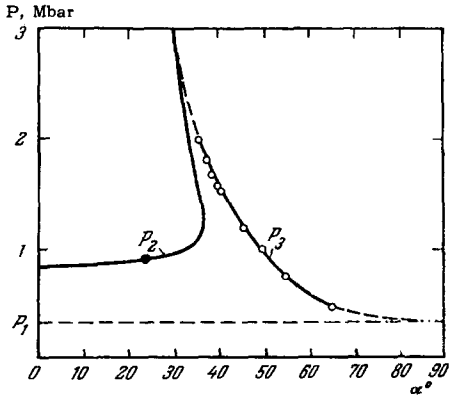

FIG. 39. Pressures due to the collision of shock waves in aluminum[108]. 2α – angle between the fronts of the colliding waves $P_1 = 0.33$ Mbar – pressure of incident waves; P_2 – pressure of regular mode; P_3 – pressure in the case of irregular reflection behind the front of the frontal wave; ● – experimental point from[104]; ○ – experimental points from[108].

The equality of the pressures and of the tangential components of the velocities in regions 2 and 3, suggested by the elementary theory, makes it possible to calculate the parameters of double compression in region 2 from the velocity of motion of the frontal wave, i.e., from the parameters of region 3.

Unfortunately, the interpretation of the results of the experiments is still ambiguous, inasmuch as the gasdynamic regime of flow behind the front of the colliding waves is likewise not uniquely defined.

An analysis has shown[109,108] that the simplest scheme of flow with a single tangential discontinuity cannot be applied to water-like media and to metals, inasmuch as the corresponding system of equations does not have real roots. Some estimates of the position of the second adiabat were possible only for aluminum[108].

7. SINGULARITIES OF FLOWS WITH PHASE TRANSITIONS; PHASE TRANSFORMATIONS IN IRON

One of the most interesting problems in high-pressure physics is the registration, investigation, and production of new crystalline structures formed in solids upon compression. The decrease in the interatomic distances changes the structure of the energy spectrum of solids, causing broadening and overlap of energy bands. The end result of this process in semiconductors and dielectrics is their metallization, due to the closing of the energy gap between the valence band and the conduction band. The resultant metallic phases have as a rule a large symmetry and a high density. The transition under the influence of pressure to new denser crystalline structure occurs without a radical change in the nature of the chemical bond. Denser phases can arise also as a result of changes in the electron distribution, without realignment of the crystal lattice.

Such processes occur, in particular, when s-elec-

trons of cesium and rubidium sink to the lower lying d-levels. Analogous phenomena should be expected in potassium and in the lanthanide group.

In dynamic experiments, new phases are observed if the time of transformation is appreciably shorter than the duration of action of the high pressures on the investigated sample. If this condition is not satisfied, the dynamic experiments will fix metastable phases of low pressure mixtures of equilibrium and metastable phases. These possibilities must always be kept in mind in the interpretation of the results of dynamic experiments.

The specific features of flows in the presence of phase transitions are manifest both in the compression processes and in the subsequent dilatation. These features are connected with the presence of convex sections of the compression curves in the case of first-order phase transitions, which contract to a cusp (Fig. 40a). Shock waves of the ordinary kind with a single discontinuity surface are produced at pressures $P \leq P_1$ and $P \geq P_3$. States 1 and 3 lie on the common ray 0—1—3, and in spite of the difference of the pressures, have a single propagation velocity

$$D_{013} = v_0 \sqrt{\frac{P}{v_0 - v}}. \qquad (19)$$

For the interval $P_1 < P < P_3$, direct transitions of the type 0—2 are unstable, since the corresponding wave velocities are lower than the velocity D_{013} of the wave with the smaller amplitude. The decay of the discontinuity, caused by the instability, leads to the formation of two shock fronts (Fig. 40b). Moving in front is a shock wave bearing the critical pressure P_1 of the first phase. It is followed by a phase transformation wave, which changes the crystalline structure of the medium. The width of its front, proportional to the time of transformation, characterizes the kinetics of the processes which occur within a ten-millionth of a second. The velocity of the first wave is constant, while that of the second (in the laboratory coordinate system),

$$D_2 = U_1 + D_{12} = U_1 + v_1 \sqrt{\frac{P_2 - P_1}{v_1 - v_2}}, \qquad (20)$$

depends on the magnitude of the applied pressures P_2. Its upper limit is determined by the inclination of the ray 0—1—3, and the lower one by the derivative of the curve near the point 1. As the shock fronts pass in succession, the medium experiences a stepwise compression in two stages. Formulas (18) relate the thermodynamic parameters of the final state with the velocity jump ΔU_{12} of the second shock transition and the relative velocity of its propagation D_{12}. In addition to point 1, the shock-transition curve has two other kinks—in the states 1′ and 3. The former limits the region 1—1′ of the partial transformation. In this interval of pressures, the second adiabat coincides with the phase-equilibrium curve. At point 3 a change takes place in the character of the compression—from stepwise to single, leading to a larger increase in the entropy. When a shock wave of some amplitude enters into a sample that experiences phase transformation, the states first to be realized are those from the metastable branch of the adiabat of the initial crystalline phase, for example 2′ or 4′ (see the pressure-velocity diagram on Fig. 41).

The decrease in volume during the course of

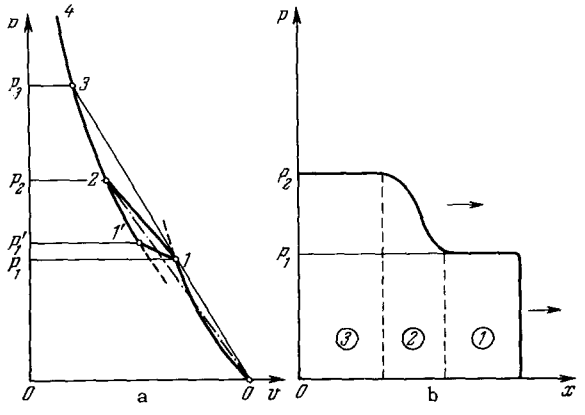

FIG. 40. a) P-v diagram of shock compression in the presence of phase transformations. 0 – 1) shock adiabat of first phase; 1 – 1′) region of coexistence of two phases; 1′ – 4) adiabat of high-pressure phase; 1 – 3) region of existence of two frontal configurations. b) Structure of shock waves accompanied by phase transformations: 1) region of location of the first phase; 2) transformation zone formed of a mixture of two phases: 3) region of completed transformation.

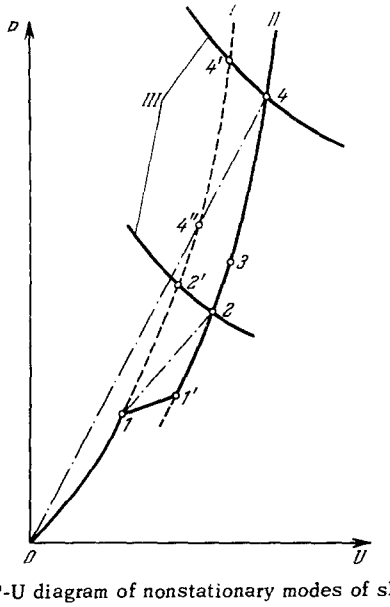

FIG. 41. P-U diagram of nonstationary modes of shock-wave motion. I – Shock adiabat of low-pressure phase, the dashed line shows its metastable section; II – adiabat of denser phase of high pressure; III – curves showing the variation of the pressures on the boundary of the sample experiencing phase transformation; 4′, 2′ – initially arising states of shock compression on the adiabat of the first phase; 4, 4″, 2, and 1 – states characterizing the stationary process of propagation of shock waves with amplitude P_4 and P_2 (see Fig. 40).

transformation leads to a decrease in pressures both on the wave front (points 1 and 4″) and on the layers of material which have gone over completely into a more dense modification (points 2 and 4). The relaxation of pressures on the fronts of the shock wave, on the initial section of its motion, is one of the clearest attributes of phase transformations in progress.

As applied to phase transformations, the elementary theory of stationary flows described above was developed by Bancroft, Peterson, and Minshall [110] and later by Duff and Minshall [111].

In many respects, the exposition in [111] coincides with Zel'dovich's theory [32] of the motion of shock waves in gases with delayed excitation of degrees of freedom. Non-stationary processes were considered qualitatively by Wackerle [112], by Kormer et al. [55], and by Ivanov, Novikov, and Divnov [113].

A great many investigations have been devoted to the high-pressure phase of iron, observed in dynamic experiments. As already indicated (see Fig. 34), explosive pressures inside steel blocks give rise to sharply delineated zones, which differ from the rest of the metal mass in the etch coloring, increased hardness, and fine-needle crystalline structure. These effects, which the author has encountered in the middle Forties, were described in detail in the thorough monographs of Rinehart and Pearson [114] and Jackson [105], in the article of Tarasov, Speranskaya and the author [104], and in many other papers. The appearance of dark zones was for a long time incorrectly attributed [114,104] to dynamic work hardening of the metal as a result of very intense twinning. In 1955, Bancroft, Peterson, and Minshall [110] observed at 130 kbar a kink in the shock adiabat of iron, evidencing a transition of this metal to a

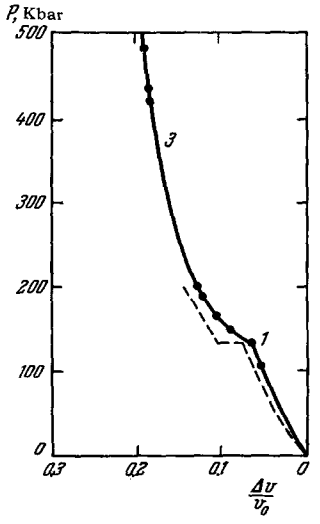

FIG. 42. P-v diagram of shock compression of iron in the region of the phase transformation, after Bancroft et al.[110] P_1 = 130 kbar – critical transformation pressure; P_3 = 330 kbar – pressure for reconstruction of single discontinuity surface.

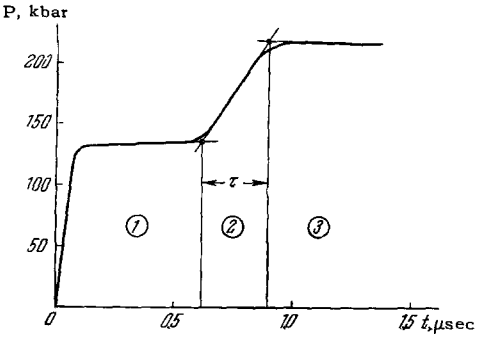

FIG. 43. Two-wave configuration in iron[113]. The smearing of the second wave front (~ 0.2 μsec) determines the time of phase transformation.

denser crystalline modification.

The profile of the two-wave configuration was obtained by the authors after a careful registration of the speed of motion of the free surface of a sample subjected to the action of explosive pressures.

The registration was with the aid of a large number of electric contacts installed on the path of motion of the surface. Using this method, the authors determined from the amplitude of the first shock wave the critical pressure of the phase transition, and from the subsequent velocity jumps they determined a series of points on the adiabat of the second phase. The results obtained by Bancroft and Peterson are shown by the solid line of Fig. 42. With the aid of more highly perfected procedure of continuous recording [116] of the speed of the boundary, the two-wave structure of a shock wave in the two-phase region of iron was recorded by Ivanov and Novikov [113] (Fig. 43). The smearing of the second shock front characterizes the time 0.2×10^{-6} sec during which the α-iron is transformed into a new phase.

In 1961 Balchan and Drickamer registered the same transformation under static conditions, by measuring at 130 kbar the electric resistance of iron. This was regarded by the authors as the phase transformation of the α structure of iron into a face-centered structure of γ-iron.

In 1962, Johnson, Stein, and Davis [117] obtained, in dynamic experiments with heated samples, the dependence of the transformation pressure on the sample temperature. They observed on the P-T diagram of the phase equilibrium (Fig. 44) at 110 kbar and 780°K a cusp, which they regarded as the triple point of the α and γ phases and a new, unknown x phase of iron. With the aid of x-ray diffraction photographs under pressure, Jamieson and Lawson [118] and finally Takahashi and Basset [14] established that the new phase has a close packed hexagonal structure. The isotherm compression obtained for iron in [14] is shown dashed in Fig. 42.

An investigation of phase transitions in iron has led Novikov and Tarasov [119,120], Erkman [121], and Balchan [122] to an experimental discovery of rare-

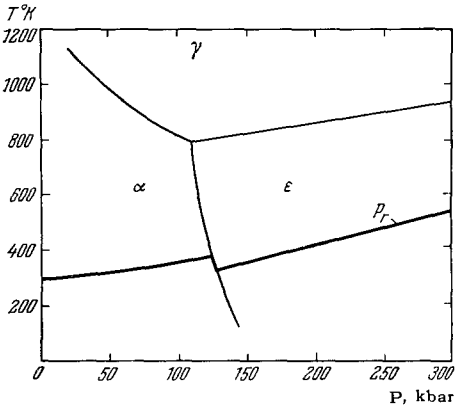

FIG. 44. Phase diagram of iron after[117] and [114]. Thin lines – phase equilibrium; thick line – shock-transition curve.

faction shock waves, which occur when the metal is retransformed when relaxed to the initial phase. In experiments of [119-120], the collision of the expansion shocks has led to unique phenomena involving smooth ruptures of the metal.

As was shown by Drummond [123] and in greater detail in [121] and [120], rarefaction shocks occur when the expansion process includes convex sections of isentropes or kinks on the isentropes (Fig. 45). An attempt to construct under these conditions simple waves without discontinuities leads to the formation of two intersecting families of characteristics, i.e., to a non-uniqueness of the solutions.

As in the case of compression waves, rarefaction shocks are stable if the velocity is supersonic with respect to the initial state and subsonic with respect to the final state. This requirement is satisfied if

$$-\frac{\partial P}{\partial v}\Big|_{v=v_1} < \frac{P_2-P_1}{v_1-v_2} < -\frac{\partial P}{\partial v}\Big|_{v=v_2}. \qquad (21)$$

The maximum amplitude of the rarefaction shock is determined by the points of tangency c and d. At smaller initial pressures, for example P_1, states can be attained as a result of the shock, lying in the

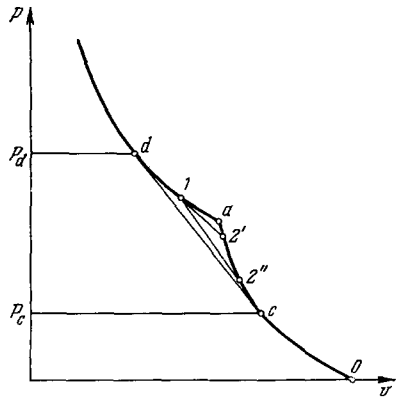

FIG. 45. P-v diagram of rarefaction shocks after[120]. 1 – initial state; 2′–2″ – interval of possible final state; $P_d - P_0$ – maximum amplitude of the rarefaction shock.

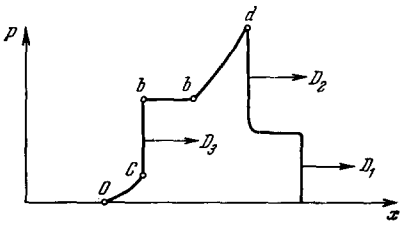

FIG. 46. Form of shock pulse containing compression and rarefaction jumps after[120]. D_1) compression shock wave of the first phase; D_2) phase transformation wave; d – b) preceding rarefaction wave; b – c) rarefaction shock; c – 0) succeeding rarefaction wave.

interval 2″–2′. The line 1–2′ is tangent to the compressibility curve at the point 1, while the line 1–2″ at the point 2′. Upon expansion to pressures lower than $P_{2''}$, a simple rarefaction wave follows the shock. If the final pressure exceeds $P_{2'}$, the simple wave precedes the rarefaction shock. The same occurs always when $P_1 > P_d$.

The profile obtained in [120] for the wave propagating through steel samples at explosion loads is shown in Fig. 46. It is made up of two shock compression waves, a rarefaction shock, and two simple rarefaction waves. Under the experimental conditions of [120], the rarefaction shocks were produced in relaxation waves traveling from the free boundary of the sample and from the side facing the charge. The trajectories of the shocks are shown on the x-t diagram of Fig.47.

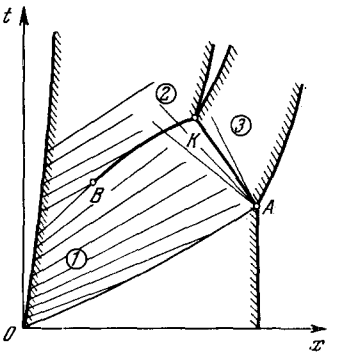

FIG. 47. x-t diagram of interaction of rarefaction shocks. OA – trajectory of shock waves in the partition; AK and BK – trajectories of rarefaction shocks.

At the point of intersection of the discontinuities of K, interaction took place between states 2 and 3 (Fig. 8), which had essentially different translational velocities. The rupture of the sample took place under the influence of tremendous negative pressures P_4 produced in the collision plane. The smoothness of the rupture (Fig. 49), of a quality similar to that obtained by working on a lathe, is evidence of the smallness of the rarefaction front width, which did not exceed several thousandths of a centimeter. The rise time of the rupture stresses was equal to several billionths of a second.

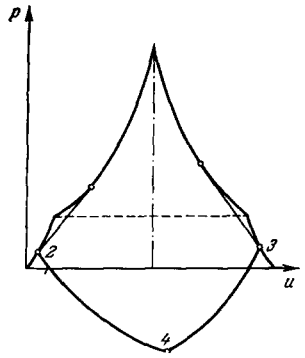

FIG. 48. P-U diagram of interaction of rarefaction shocks.

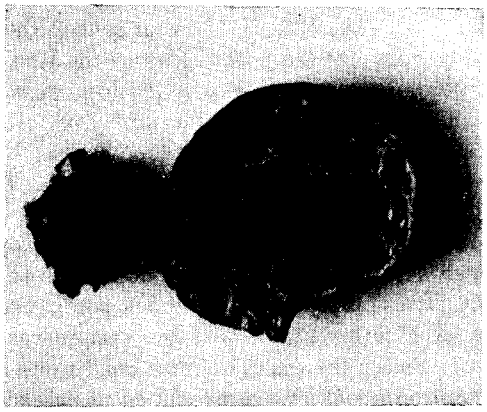

FIG. 49. Exterior of smooth cleavage surfaces where rarefaction shocks meet.[19]

8. EQUATIONS OF STATE AND PHASE TRANSFORMATIONS OF IONIC CRYSTALS

According to generally accepted premises, the ions of the electropositive and electronegative elements which make up the lattice of ionic crystals are bound together by Coulomb attraction forces. These are opposed by short-range repulsion forces between the contiguous electron shells. For large readily-polarizable ions, an appreciable role is played by the Van der Waals forces.

Along with theoretical calculations of the interaction forces, independent interest attaches to their experimental determination by recording the pressures under different degrees of compression. No less important is an investigation of the thermodynamics of the crystal lattice of ionic crystals, since a study of their properties is complicated at high temperatures, as in the case of metals, by the presence of a free electron gas: the appearance of such a gas is hindered by the wide energy gap that separates the conduction and valence bands.

The isotherms obtained by Bridgman [7] for many ionic compounds are known up to pressures of 100 kbar. An outstanding most recent attainment is the x-ray diffraction registration of the isotherm of CsCl up to 500 kbar by Drickamer et al [124].

Dynamic methods were used to investigate the most typical representatives of the ionic compounds, such as the halides of alkali metals. In the first two investigations of Pavlovskiĭ, Kuleshova, Simakov, and the author [63,53] dynamic adiabats were obtained for NaCl, LiF, KCl, KBr, NaI, and CsI up to 1 Mbar. Results in the same pressure range—up to 800 kbar for NaCl and up to 300 kbar for KCl and CsI—were reported by Christian and Alder [29].

In an appreciably larger pressure interval, of several megabars, the shock compression of solid and porous samples of LiF, NaCl, KCl, KBr, and CsBr was investigated by Kormer, Sinitsyn, Funtikov, and Urlin [55]. Analogously, CsI was investigated in [125].

Extension of the research, with the aid of shock experiments, into the region of high pressures and compressions, has made it possible to determine more accurately the ion pair interaction potential, represented in [63,53] in the form of a Coulomb attraction potential $\sim e^2/r$ and an exponential Born-Mayer repulsion potential [64]

$$\sim e^{-\frac{r}{\lambda}} = e^{-q\frac{r}{r_{0k}}}$$

($q = r_{0k}/\lambda$, r_{0k}—distance between ions at $P = 0$ and $T = 0°K$). The parameter λ in the argument of the exponential characterizes the degree of smearing of the electron shells.

The pressures (15) and the energy (15a) of cold interaction (Sec. 2) in the case of a two-term potential of this type contains only one free parameter q. The second coefficient in (15) is determined for ionic crystals from general-physical constants, the Madelung constant, and the equilibrium inter-ion distance r_{0k}. The true values of q were obtained in [63,53] by comparing the experimental and calculated adiabats, plotted for different q using Eqs. (15) and (9) for $P_c(v)$, $E_c(v)$, and $\gamma(v)$. The results of the analysis for six ionic crystals (LiF, NaCl, NaI, KCl, KBr, CsI) are given in the upper lines of Table V. They were obtained in [125] for CsI using a more accurate potential that includes the Van der Waals forces. The parameter $\lambda = r_{0k}/q$ is not the same for the different salts. Its value increases linearly with increasing interionic distance r_{0k}.

As shown in Table V, the least compressible at 1 Mbar is lithium fluoride, followed by sodium chloride, which occupies an intermediate position. The remaining salts have a larger and approximately equal compressibility. This tendency remains also when higher pressures are applied, such as used in [55,125]. At a pressure of 4 Mbar the density of LiF increases by a factor 2.12, that of NaCl by 2.90, and that of CsBr, KCl, KBr, and CsI by 3.0—3.3 times.

Great differences are observed in the shock-compression temperatures calculated in [53,125] (see Table V). For LiF at 1 Mbar they are equal to 0.28 eV, or 5% of the half-width of the forbidden band, while the value for CsI is 2.28 eV, or 75% of the value of $(1/2)\epsilon_0$. In the case of CsI, the number of electrons

Table V. Parameters q and λ and characteristics of shock compression of ionic crystals at pressure 1 Mbar (*) and 4 Mbar (**) from [53,55] and [125].

Substance	LiF, r_{0k}=1,996 Å	NaCl, r_{0k}=2,794 Å	KCl, r_{0k}=3,251 Å	KBr, r_{0k}=3,427 Å	NaI, r_{0k}=3,198 Å	CsI, r_{0k}=3,905 Å
q	7.6	9.2	10.0	10.0	9.7	10.0
λ, Å	0.263	0.304	0.325	0.343	0.330	0.390
ϱ/ϱ_0^*	1,57	1.91	2.09	2.16	2.05	2.10
T^*, eV	0.28	0.78	1.53	1.80	1.46	2.28
$2T^*/\varepsilon_0$	0.049	0.22	0.41	0.55	0.54	0.76
ϱ/ϱ_0^{**}	2.12	2.90	3.19	3.31		3.00

transferred to the conduction band is already comparable with the number of ions at these pressures in order of magnitude.

To illustrate the isothermal compressibility and the differences in the courses of the isotherms and the shock adiabats, Figs. 50 and 51 show plots of $P_C(\sigma)$ and $P_H(\sigma)$ for NaCl and CsI.

Abundant experimental material, characterizing the thermodynamic properties of ionic compounds at the highest temperatures, was obtained by Kormer, Funtikov et al.[55] by compressing porous samples of NaCl, LiF, and CsBr. Similar experiments were made also on CsI[125].

Figure 50 shows a comparison of the experimental points of porous adiabats from [55] and the calculated dynamic adiabats (dashed) plotted in the harmonic-oscillator approximation. They are in patent disagreement with experiment. Agreement according to [55] is attained only after the influence of anharmonicity is taken into account. In the present review, the adiabats represented by the continuous lines have been calculated by the "free volume" theory using the equation of state for NaCl from [53].

The use of the free volume theory has made it possible to represent in [53] the thermodynamic functions in the form of universal functions of dimensionless temperatures and densities. This simple result was obtained for ionic crystals as a result of the dropping out of the Coulomb forces in the free-volume theory approximation (the Coulomb forces are identically equal to zero in the symmetrized field of spherical cells). As noted in Sec. 2, the free volume theory makes it possible to describe, if the interaction potential is specified, the influence of anharmonicity of thermal oscillations and the gradual acquisition on the part of the oscillating ions of the thermodynamic characteristics of an ideal gas with increasing temperature. The fact that the experimental dynamic adiabats of NaCl swing to the right of their dashed positions is a clear cut manifestation of this process. For CsI and CsBr salts, which

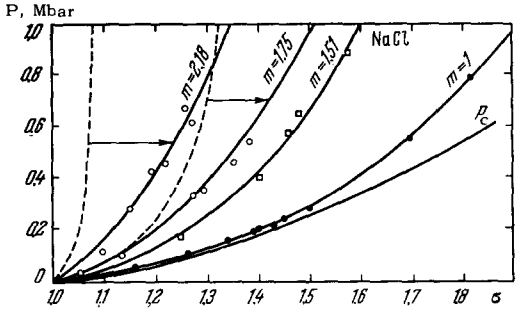

FIG. 50. Shock adiabats of sodium chloride of different porosity. ●– data of Al'tshuler, Pavlovskii, and Kuleshova[63]; o – data of Kormer, Funtikov, et al.[55]; □ – experimental points obtained by the authors of[125]; – – – calculated adiabats constructed in the harmonic approximation; – – adiabats calculated from the equation of state proposed in[53]; reduction in the specific heat and the Gruneisen coefficient of the lattice with the temperature are described by the "free volume" theory.

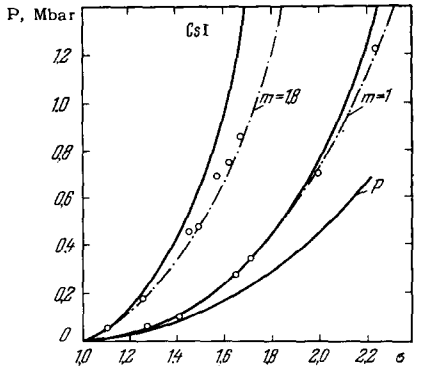

FIG. 51. Zero isotherm and dynamic adiabats of CsI[125]. – – adiabats calculated with account of anharmonicity by the "free volume" theory; –.–.– – calculation which takes additional account of the contribution of the thermally excited electrons.

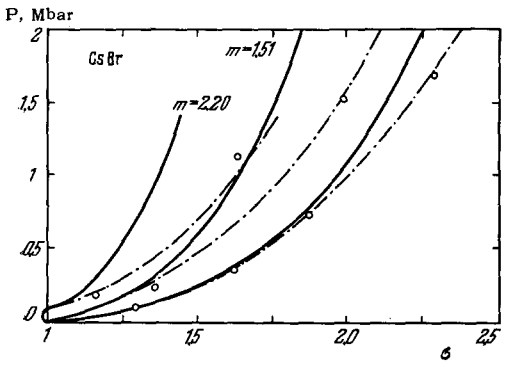

FIG. 52. Dynamic adiabats of CsBr[55]. – – adiabats calculated with account of anharmonicity; – . – – calculation which takes additional account of the thermally excited electrons.

have a large molecular weight and in which the shock-compression temperatures are especially large, the agreement between calculation and experiment, as shown in Figs. 51 and 52, is attained [55,125] only by introducing into the equation of state the electronic terms that describe the excitation of the electrons and their transition to the conduction band.

The initial stages of this process, as well as ionic conductivity phenomena, can be experimentally established by measuring the electric conductivity behind the shock-wave front.

The sharp increase, by many orders of magnitude, in the conductivity of the explosion products and of some other organic compounds following the passage of detonation and shock waves was observed by Brish, Tsukerman, and Tarasov [126]. Analogous phenomena were registered by Alder and Christian [127] in CsI, LiH, and teflon. In [127] this effect was initially attributed to metallization of substances by closing of the energy gaps between the valence bands and the conduction bands.

In an already cited paper [63], the measured conductivities in NaCl were set in correspondence with the shock-compression temperatures. The activation energy obtained in this fashion, ~1.2 eV, is close in magnitude to the activation energy characteristic of ionic-conductivity processes. By way of an alternative, this same activation energy can be regarded in accordance with [29] as a characteristic of electronic processes for which the number of carriers is $n \sim \exp(-\epsilon/2kT)$. This interpretation yields, from the same experimental data, a value $\epsilon \sim 2.5$ eV. For several other salts, the values of ϵ obtained by Alder [29] are listed in Table VI. All differ noticeably from the values of ϵ_0 for normal conditions.

The great reduction in the effective dimensions of the energy gap can occur both as a result of broadening of the bands upon compression, and as a result of temperature effects due to electron-phonon interaction [29]. On the whole, the question of the nature of the conductivity of shock-compressed ionic crystals is at present far from clear.

Table VI. Dimensions of forbidden bands of ionic crystals in the normal state (ϵ_0) and behind the front of the shock wave (ϵ) of amplitude P. The values of ϵ were calculated in [29] from measurements of the conductivity.

Compound	$P_{k\delta}$	ϵ, eV	ϵ_0, eV
NaCl	220	2.4	8.4
KI	160	4.1	
CsI	190	4.7	6.3
CsBr	270	4.3	7.0
CsCl	270	4.3	7.7

Pressures cause a transition to closer packing of the ions in ionic crystals and give rise to structures with larger values of the coordination number (c.n.).

Similar transformations in crystals with structures of the NaCl c.n. type (i.e., the number of nearest neighbors is equal to 6) into a structure of the CsCl type with body-centered lattice (c.n. = 8) were observed by Bridgman in halides of potassium and rubidium. The specific volume in the transformation process decreased by 14—16%. The results of static and dynamic experiments on KCl and KBr are compared in Fig. 53. The curves show that in this case the transition to conditions of dynamic deformation did not change the phase-transformation pressures. A kink is observed at the same pressure, 20 kbar, on both the isotherms and the shock adiabats.

The question of the phase transformation in rock salt, for which the coordination number 6 is certainly more stable under normal conditions than for KCl and KBr, was debated for a long time. According to quantum-mechanical calculations by Lovdin [128] the initial NaCl structure remains stable up to pressures of 90 kbar. In Bridgman's experiments, no phase transformations were observed up to pressures of 100 kbar, and in the case of shock compression (in [63]) up to 800 kbar.

The formation of a body-centered crystal structure in NaCl was first disclosed by Evdokimova and Vereshchagin [129,130] using x-ray diffraction photo-

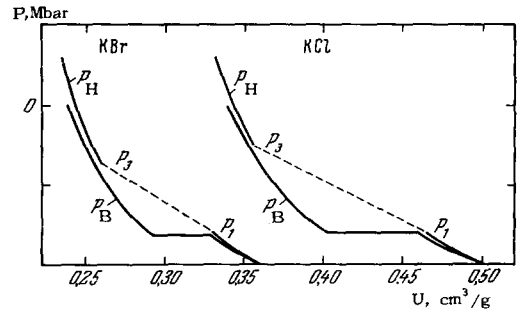

FIG. 53. Static and dynamic diagrams of phase transitions in KCl and KBr (from[53]). P_B – Bridgman's isotherms, P_H – shock adiabats.

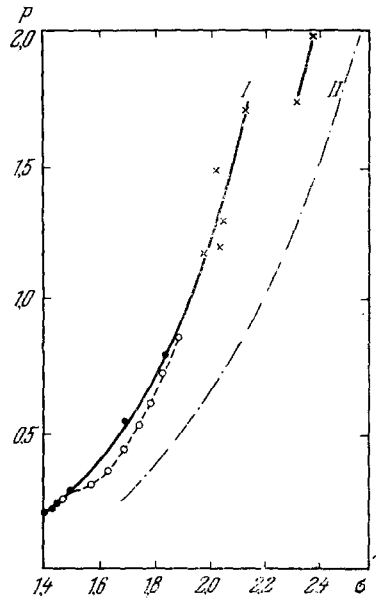

FIG. 54. Shock adiabats of sodium chloride from[63, 29] and[55]. I and II – Calculated adiabats of low and high pressure phases; ● – experimental data from[63]; o – data by Alder[29]; x – from[55].

graphs under pressure. As a result of application of 20 kbar for many hours, up to 5% of the substance was converted into a new phase with CsCl structure.

Unlike in [63], Alder [29] noted at pressures above 300 kbar a shift in the compression curve (shown dashed in Fig. 54) towards the denser phase. The disagreement with [63] may be due to the different sample sizes used in the experiments, for samples of larger dimensions make it possible to register later stages of the transformation process. To check on this assumption, the authors of [63] undertook special experiments in which they registered the parameters of the shock wave in NaCl as the latter propagated through the sample. They measured in the experiments the flight velocity of thin and light plates of polyethylene ($\rho_0 = 0.9$ g/cm^3) attached to salt samples of different thickness. From the plate velocities they determined the minimum pressures of the leading boundary of the front. The upper curve of Fig. 55 was plotted from the results of control experiments on aluminum samples. The curve (111) characterizes the small attenuation of the shock wave of 400 kbar amplitude moving in NaCl single crystals in the direction of the diagonal axis. The most intense pressure relaxation, and consequently the most intense phase transformation reaction, occurs for shock compression in the direction of the edge of the cube [curve (001)]. On the whole, the experiments confirmed the presence of the very start of the transformation process, but did not lead to quantitative agreement with [29]. In direct contradiction of [29] was also the effect of the crystallographic orientation.

Very interesting results were obtained by Kormer,

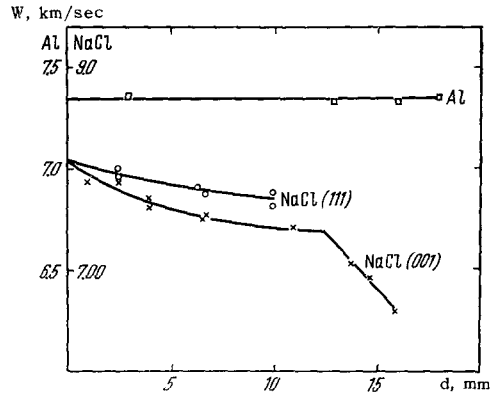

FIG. 55. Relaxation of pressures on the front of shock waves in samples of rock salt. W – velocity of plate of polyethylene, characterizing the pressure on the forward boundary of the shock front; d – thickness of sample; □ – results of control experiments on aluminum samples; o – data obtained for a shock wave moving in the direction of the diagonal of a cube; x – in the direction of the edge of the cube.

Sinitsyn, Funtikov et al.[55], who registered at ~1.5 Mbar the states of different density in the NaCl liquid phase (upper area in Fig. 55). As is well known the melting of crystalline bodies does not signify a transition to a random distribution of the atoms of ions, but only the loss of far-range order in their arrangement. If the potential energy difference between two competing coordinations is much smaller than kT, then the liquid consists in the equilibrium state of configurations of both types, and furthermore in approximately equal amounts.

Less dense states of liquid NaCl correspond, in accordance with [55], to an initial non-equilibrium structure of a "lattice" liquid with a coordination number equal to 6 uniformly over the entire volume, while denser states correspond to an equilibrium state of a mixture of two coordinations, with 6 and 8 neighbors.

9. TRANSITIONS TO THE METALLIC STATE

The pressures at which insulators turn into semiconductors and metals is determined by the width of the energy gap separating the filled valence band from the conduction band. The gap size depends in turn on the relative electronegativity of the elements making up the compound.

The largest gap, 5—11 eV, is observed in halides of alkali metals. In the experimentally accessible region of shock pressures for such halides, we can speak only of "temperature metallization" due to the transition of a large number of electrons to the conduction band, induced by thermal excitation.

The compression of these crystals is insufficient by itself to close the gap, and according to the theoretical calculations made in [131] for CsI it does not even lead to a decrease in the gap. For lithium hy-

dride, according to [132], the metallic state is reached at 24 Mbar.

Of great interest is the question of the transition to the metallic phase of molecular crystals, primarily hydrogen. According to Abrikosov [133], metallic hydrogen is stable at 2 Mbar. Owing to the low initial density of the hydrogen, these pressures cannot be produced with the aid of shock waves.

The molecular structures of halides are more convenient for investigation. In particular, in the case of iodine, according to Alder and Christian [134,29] the breaking of the directed valence bonds and the formation of an atomic metallic structure occur at pressures of 700 kbar.

Theoretically, the transition to the metallic state was predicted by Gandel'man [135] for argon as a result of the transition of its p-electrons to the lower level of the d-band. However, as shown by Alder et al.[59], the dynamic adiabat of argon has no singularities whatever up to 500 kbar.

A large number of transformations, accompanied by the occurrence of metallic conductivity, was observed in static experiments for elements of groups III—V and their compounds, i.e., substances in which the width of the forbidden energy band is 0.8—2.0 eV [136].

The best known example in which metallic properties are acquired under pressure is the transformation of red phosphorus into the black modification. The transition occurs at 70 kbar under static conditions and at somewhat lower pressures, 25—35 kbar, under dynamic conditions.[29] The reasons for this decrease in pressures lie, according to [29], in the presence of shear deformation (see Sec. 11).

We shall discuss in greater detail the results obtained with the aid of shock waves in the study of the equations of state of silicon and carbon.

Silicon in the initial state has a density 2.33 g/cm^3, is a semiconductor, and crystallizes with a firm but not close-packed diamond structure: as is well known, the atoms occupy only 34% of the total volume of cells in the three dimensional diamond lattice.

Drickamer and Mikomura found [10] static compression of silicon to 195—200 kbar increases its electric conductivity by 10^5—10^6 times, to that of aluminum. This circumstance is undoubtedly evidence of the transition of silicon into the metallic state. They have also observed that under conditions of shear deformation, the same process occurs also at noticeably lower pressures, 150—135 Mbar.

As shown by the x-ray structural investigations of Jamieson [137], silicon crystallizes under 160 kbar pressure into a tetragonal structure of gray tin with density 3.37 g/cm. The metallic properties are partially retained also after removal of the pressure. According to Kasper and Wentorf [138] the crystal modification produced upon relaxation has cubic symmetry and a density 2.55 g/cm^3.

Pavlovskiĭ and the author investigated the silicon system up to 2 Mbar shock pressures which increased its density to 4.5 g/cm^3. To register the lower section of the shock-compression curve, the experiments were carried out by the magneto-electric procedure described in Sec. 3. This yielded a continuous record of the velocity of the boundary of the silicon sample with a paraffin block. The series of oscillograms reproduced in Fig. 56 demonstrates the form of the multi-wave configuration produced when shock pulses with different amplitudes pass through the silicon plate. The shock-transition curve reproduced from these records, in Fig. 56b, has two distinct kinks. The first is due to the transition of silicon from the elastic state to the plastic one. The second kink at 100 kbar is connected with the onset of conductivity and with the initiation of the manifestation of a new phase.

Another group IV element, carbon, was investigated in detail by Alder and Christian [139] (Fig. 57).

The lower section of the diagram, up to 100 kbar, characterizes the compression of the graphite. In the interval from 100 to 400 kbar, nonequilibrium states of the mixture of two phases are realized, while the diamond phase prevails above 400 kbar. In the opinion of the authors of [139], the upper points of

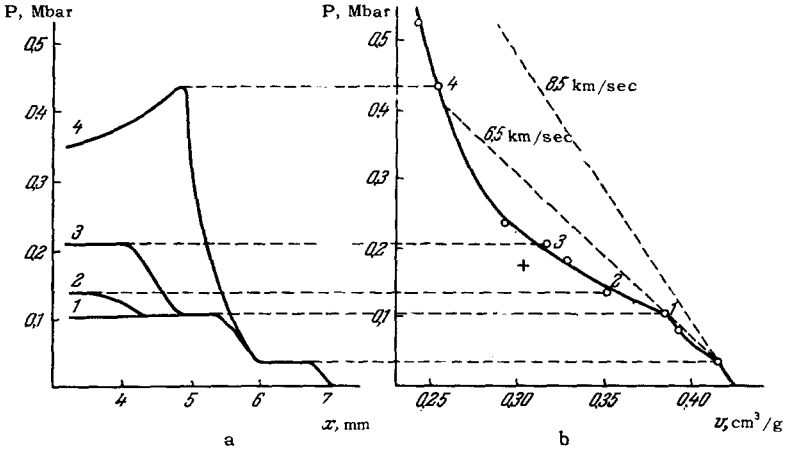

FIG. 56 a) Multi-wave configurations arising when shock pulses of different amplitudes pass through silicon samples; b) curve of shock compression of silicon. – – wave lines corresponding to wave velocities 8.5 and 6.5 km/sec; 1 – 4) states fixed by magneto-electric measurements; + – experimental point of Jamieson[137].

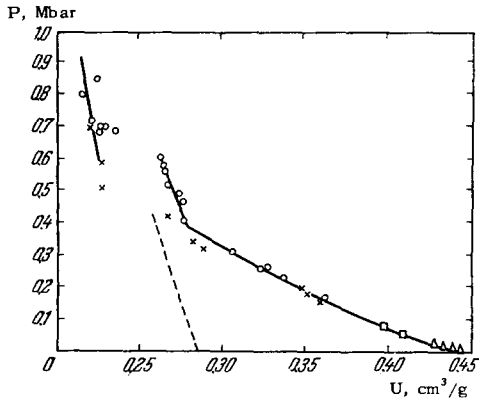

FIG. 57. P-v diagram of compression of graphite by shock waves, after Alder and Christian[139] o – initial density of samples $\rho_{00} = 2.14$ g/cm³; × – initial density $\rho_{00} = 1.7$ g/cm³; – – – compression curve of diamond.

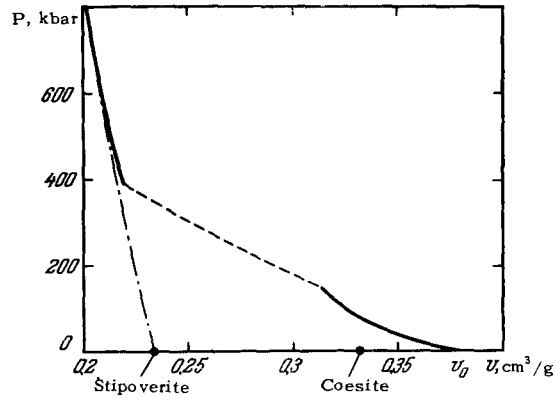

FIG. 58. P-v diagram of compression of quartz by shock waves, after Wackerle[112].

the diagram pertain to the metallic state of carbon.

It is remarkable that the diamond formation process, which under static conditions necessitates many hours of exposure to high pressure, was completed within a fraction of a microsecond, i.e., within a time interval shorter by a factor 10^{10}.

We can expect[140,141] the use of high explosion pressures for the acceleration of chemical reactions to lead to the appearance of a new scientific discipline—the chemistry of superhigh pressures.

10. ON THE COMPOSITION OF THE EARTH'S CORE AND THE MANTLE

The structure of the earth's sphere and the distribution of pressures and densities along the earth's radius have been determined by now with sufficiently high reliability.

The basic information on the internal structure of the earth was obtained by recording the velocities of seismic waves at different depths. It was established in this manner that there exists a heavy liquid core with a small solid sub-core and a solid and lighter silicate shell—the earth's mantle, separated from the earth's crust by the Mohorovicic boundary. According to contemporary notions (Birch[142], Ringwood[143], Stishov[144]) the main components of the mantle are minerals of the type of olivine [$(MgFe)_2SiO_4$] and enstatite [$(MgFe)SiO_3$], which undergo a series of phase transformations in the upper part of the mantle, the so-called C layer. The final link in these transformations is the formation of the corundum modification of enstatite, periclase (MgO), and "stipoverite," the most compact oxide of silicon with density 4.3 g/cm³ at atmospheric pressure. Discovery by Popova and Stishov[145] of this densest form of quartz has played an important role in the development of correct notions concerning the composition of the earth and of planets of the earth group.

The authors of[145] observed stipoverite in the form of a metastable phase by compressing quartz to 160 kbar and heating it to 1700° C. Subsequently stipoverite was found in the crater of an Arizona meteorite. It is probable that it was formed there as a result of impact of the meteorite against the quartz-containing mountain rocks. Favoring this hypothesis is the shock adiabat of quartz, obtained by Wackerle[112] (Fig. 58). The course of the upper section of the adiabat corresponds to compression of its densest phase—stipoverite.

The development of dynamic methods has made it possible to check experimentally various points of view concerning the composition of the mantle and the core. The first studies of mountain rocks—dunite and gabbro—up to pressures of 700 kbar were made by Hughes and McQueen[146].

Great interest attaches to the compression curves of minerals in the ranges of the higher pressures of the lower mantle and the core. Investigations of this kind were made by Trunin, Gan'shikova, and the author for 15 mountain rocks and for several minerals. Some of these results, together with data published previously[147], are shown in Fig. 59, which

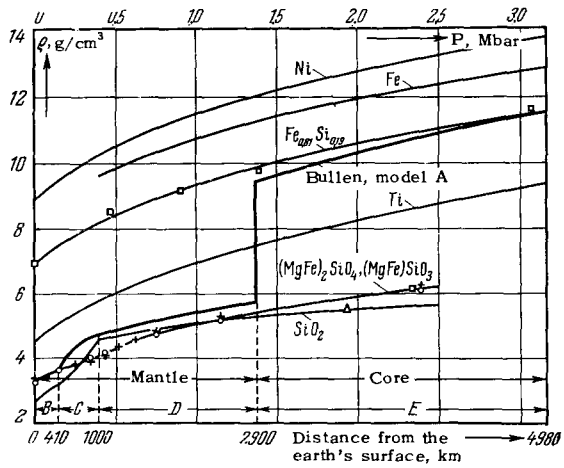

FIG. 59. Adiabats of shock compression of metals and minerals, and P-ρ diagram of the earth.

shows also the adiabat of silicon iron obtained by Kormer and Funtikov [148], and the adiabats of iron and nickel [36,39,42] and titanium [43].

The abscissas of the diagram are the pressures and the corresponding distances from the earth's surface, while the ordinates are the densities. As shown by the diagram, the shock adiabats of forsterite, enstatite, and most other magnesium silicates lie parallel to the compression curve of the lower mantle, at a distance of 0.3 g/cm^3 in the direction of the ordinate axis. This discrepancy increases somewhat after corrections are introduced for the difference between the temperatures of the earth's mantle and shock compression. The agreement between the experimental compression curves and the Bullen curve for the lower mantle should occur in the case of iron-magnesium silicates containing ~15—20% iron by weight.

The hypothesis with the largest number of adherents is that the earth has an iron-nickel core. Contradicting it are the views of Lodochnikov [149] and Ramsey [150], who believe that the earth has a uniform chemical composition and that the core is made of metallized silicates. This hypothesis is based on the notion of the phase transformation of the densest crystalline forms of iron-magnesium silicates of the lower mantle into even denser metallic states of the liquid core.

In spite of the fact that from the crystal-chemistry point of view the attainment of such silicate-based metallic states has very low probability [143], these views still find adherents to this day, and not only among astronomers [151] but also among geochemists [144]. Dynamic experiments did not confirm the hypothesis of Lodochnikov and Ramsey. The experimental points obtained at pressures 2—2.5 Mbar on the shock adiabats of quartz, forsterite, and enstatite lie at densities which are almost half the density of the earth's core (see Fig. 59).

It is difficult to judge at present the extent to which this result can be undisputedly related to terrestrial conditions, since the geological time scale differs from the time scale of explosion experiments by more than 22 orders of magnitude. Comparison of the adiabats of iron and nickel with the $P - \rho$ diagram of the earth's core shows that the core cannot consist of iron alone or of its alloy with nickel. According to the experimental data of Kormer and Funtikov [148], agreement with the Bullen model can be attained by introducing into the composition of the iron core some 15—20% of silicon by weight. The same result can be obtained also by adding oxides or sulfides [147] of iron.

The question of a core consisting of iron alone was considered by Zharkov [152]. This point of view leads, however, to unrealistically high temperatures in the earth's center, ~11 × 10^3 °K.

Some of the deductions given here were drawn earlier in [147], and with respect to the composition of the core also in the paper by Knopoff and MacDonald [153]. The latter based their conclusions on experimental data obtained in the Soviet Union on shock compression of iron and other metals. [36,38].

11. DYNAMIC STRENGTH OF MATERIALS

The most universal example of realignment of the crystal lattice under the influence of shock waves is the transition of a substance from the elastic state into the plastic one. This transition has all the characteristic features of phase transformations in shock waves. Its study yields the dynamic ultimate strengths of metals at extremely large deformation velocities.

Macroscopically, the deformation of the medium behind the shock-wave front remains uniform. Within the limits of elasticity, a similar character of unilateral compression is exhibited also by the deformation of the atomic space lattice, shown in a highly exaggerated form [154] in Fig. 60a.

At large degrees of compression, the thermodynamically most convenient is symmetrical deformation of the unit cells under the action of hydrostatically stressed states. The transition to such a state is connected with a realignment of the crystal lattice and forced migration of the atoms from layer to layer.

A possible structure of the transition zone [154], comprising the front of the waves, is shown schematically in Fig. 60b. Its real width is not known at present. Nor have the crystallographic aspects of this unique process of cold recrystallization—the dimensions of the newly formed crystal blocks and their orientation relative to the "parent" crystals—been investigated.

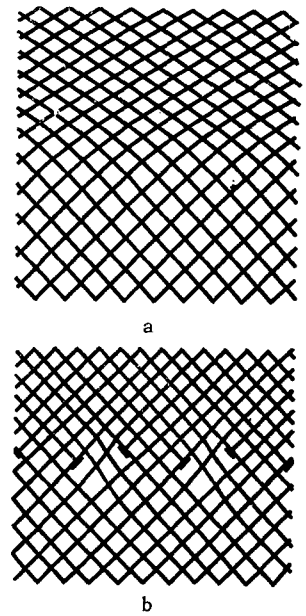

FIG. 60. Boundary of shock wave for elastic (a) and quasi-hydrostatic (b) compression of the three-dimensional lattice, after[154].

As noted by Alder (see [29]), the realignment of the crystal lattice contributes to the transformation of metastable crystalline forms into stable modifications. This circumstance is precisely the explanation for the decrease noted in [29] in the pressures of the phase transitions of phosphorus, and possibly also of silicon.

Turning to the structure of elastic-plastic waves, let us use the P-v diagram of Fig. 61, which can be regarded as the compression diagram of crystalline bodies having a definite yield point. In the elastic states, on the section 0—1, the stresses P_r, which are perpendicular to the front of the wave, are proportional to the modulus

$$E_{el} = k + \frac{4}{3}G$$

(k—modulus of bulk compression, G—shear modulus).

So long as $P < P_r(1)$, the velocity of the shock front is close to the elastic velocity of sound

$$C_{el} = \sqrt{\frac{k + \frac{4}{3}G}{\varrho}}.$$

Above the Hugoniot yield point, the front of excess pressure with P_r slightly larger than $P_r(1)$ propagates with a velocity $C_p = \sqrt{k/\rho}$. It is obvious that $C_{el} > C_p$. The velocity ratio C_{el}/C_p depends only on the Poisson coefficient μ. For some metals the values of C_{el} and C_p are given in Table VII.

With increasing shock compression pressure, the velocity of the "plastic" shock waves increases, while the velocity of the leading elastic waves, which carry the critical pressures of the elastic limit, remain unchanged.

A two-wave configuration of elastic-plastic waves was first encountered by the author in the middle Forties in a study of the effect of explosion on steel plates. Experiments on the determination of the wave velocities in steel, performed during that period and published in [104], consisted of simultaneous detonation of charges q_1 and q_2 of different length on opposite sides of thick steel plates (see Fig. 33).

Etching of the macro-section of the ruptured plate disclosed two sharply delineated regions of darkening,

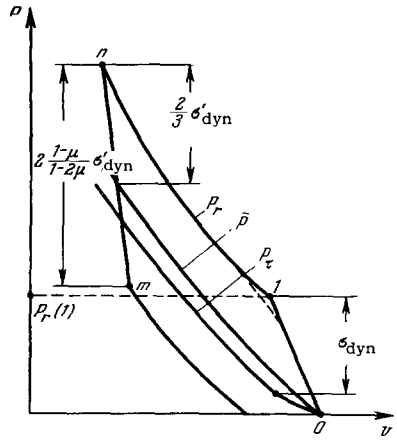

FIG. 61. Compression and relaxation curves of an elastic-plastic medium. $P_r(1)$ – Hugoniot yield point; P_r and P_t – normal stresses of compression in the direction of motion of the shock wave and in the plane of its front; $\bar{P}$ – hydrostatic compression curve; n – m – elastic stage of expansion; σ_{dyn}, σ'_{dyn} – elastic yield points at low and high pressures.

adjacent to the charges, and a narrow lens-like zone at the place where the waves met.

The velocity

$$D_M = D\frac{2\Delta M}{q_2 - q_1}$$

was determined from the velocity of detonation D and displacement ΔM of the point of collision relative to the midplane of the plate. It was found to be 4800 m/sec.

The results of the experiments have shown [104] that the main pressures of the explosion were transmitted through partitions by means of plastic waves, and that consequently the excess of the dynamic yield point over the static one is not as appreciable as would be expected for such high deformation speeds.

In the scientific literature, the two-wave structure of elastic-plastic waves was first described by Pock and Evans [155] (1948) and later by Allen (1953) [156], Bancroft, Peterson, and Minshall [110], Minshall [157] and Costello [158].

A detailed structure of these waves was registered, with experimental virtuosity, by Ivanov, Novikov, and

Table VII. Velocities of elastic and plastic compression and dilatation waves

Metals	Compression waves, $P \sim \sigma$ dyne				Dilatation waves[37]				
	C_{el}, km/sec	C_p, km/sec	ν^2	μ_0	P*, kbar	C_{el}, km/sec	C_p, km/sec	ν^2	μ^*
Aluminum	6.39	5.20	1.51	0.33	215	8.70	7.05	1.52	0.33
Copper	4.80	3.95	1.48	0.34	410	6.33	5.50	1.32	0.38
Iron	6.01	4.63	1.69	0.28	415	7.15	6.15	1.35	0.37
Lead	2.08	1.91	1.20	0.43					

P* – pressure behind the front of the shock waves.
μ^* – Poisson coefficient, calculated from the values of ν^2 using the relation $\nu^2 = 3(1-\mu)/(1+\mu)$,
μ_0 – Poisson coefficient under normal conditions.
ν – ratio C_{el}/C_p.

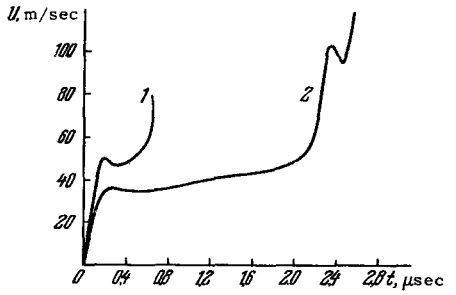

FIG. 62. Elastic-plastic waves in soft steel samples[159]. 1 – Sample 30 mm long, 2 – sample 90 mm long.

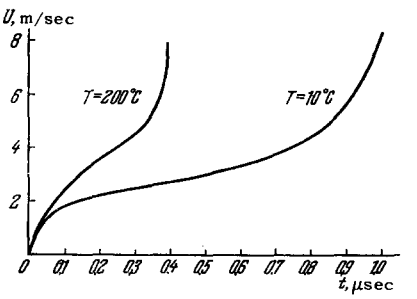

FIG. 63. Elastic-plastic waves in copper samples at initial sample temperature 10 and 200°C.

Sinitsyn [159], by Fowles [160], and by others [161,162], using new improved methods of continuous observation of the motion of the free surface of a partition from which elastic and plastic waves are reflected. The results obtained in [159] with capacitive pickups are shown in Figs. 62 and 63.

In carbon steel, the front of the elastic wave is clearly pronounced and has a characteristic analog of the ductility "tooth." In copper, which does not have a definite yield point, the leading zone is formed by a group of waves with large dispersion: their velocities are intermediate between the elastic and plastic sound velocities.

Others beside Ivanov et al.[159] who examined in detail the feature of such flows, constructed from simple waves of compression and discontinuities, were Jacquesson [105,163], Duvall [164], and in much earlier Barenblatt [165], who studied shock deformation of rods. The principal result of experimental investigations of this type is the determination of the strength of materials under conditions of superfast deformation.

By definition, the dynamic yield point is the difference between the principal stresses $P_r - P_\tau$ at the pressures corresponding to the transition to the plastic state (point 1 on Fig. 61). Under conditions of one-dimensional shock compression we have

$$P_\tau(1) = \frac{\mu}{1-\mu} P_r(1)$$

and the dynamic yield point is

$$\sigma_{dyn} = \frac{1-2\mu}{1-\mu} P_r(1).$$

The results of the determination of $P_r(1)$ and σ_{dyn} by different workers are listed in Table VIII. In order of magnitude, we have for steels σ_{dyn} ~ 5—15 kbar, and for aluminum ~ 2—4 kbar. These are much higher than the static characteristics, but still differ greatly from the theoretical strength of the metals.

The greatest increase over the static value, by a factor of several times, occurs for soft steels. With increasing static strength, the dynamic coefficient $K = \sigma_{dyn}/\sigma_{st}$ decreases monotonically.

The scatter of the experimental data in the table is due to a considerable extent to different approaches in the interpretation of the experiments. In [157,158] and [160], the pressures $P_r(1)$ were determined from the amplitude of the elastic-wave front,

Table VIII. Amplitudes of elastic waves and dynamic strength of metals

Material	Static yield point, $\sigma_{s\,0.2}$, kbar	P_r (1), kbar	σ_{dyn} kbar	$\frac{\sigma_{dyn}}{\sigma_s}$	Author
Armco iron	1.91	6.8	4.0	2.1	Bancroft[110]
Soft steel	2.12	10.7	6.5	2.9	Costello[158]
SAE-1020 steel	2.85	11.4	7.4	2.6	Minshall[157]
Aluminum alloy 2024 TU (annealed)	1.0	0.9	0.45	0.45	Fowles[160]
Aluminum alloy 2024 TU (quenched)	2.9	5.4	2.8	0.96	Fowles[160]
Armco iron	1.5	11.5	7.18	4.8	Ivanov, Novikov et al[159]
Steel 3	2.1	14.0	8.7	4.14	
Steel 40 Kh (annealed)	4.2	19.1	12.0	2.85	the same
Steel ZOKhGSA (annealed)	4.7	19.8	12.5	2.98	the same
Steel ZOKhGSA (quenched)	14.5	28.4	18.0	2.24	the same
Aluminum alloy D16 (annealed)	1.3	4.75	2.63	2.02	the same
Aluminum alloy D16 (quenched)	2.7	7.6	4.2	1.56	the same

while in [159] they were determined from the base of the elastic wave, at the boundary with the plastic region, which apparently is more correct.

In addition to metals, transitions into the state of plastic flow were fixed also in brittle metals such as copper glass [166], silicon (see Sec. 9), and quartz [112]. The maximum amplitudes of the elastic waves in these materials were 70, 40, and 35—70 kbar.

The presence of mechanical strength greatly influences the expansion of the shock-compressed materials. Materials which are in the state of plastic flow regain the ability to be elastically deformed when the direction of the deformation is changed. A similar sequence of processes is realized when the shock wave overtakes the relaxation waves that come from the rear or from the side.

In the elastic stage of expansion, the difference between the principal stresses, initially equal to σ'_{dyn}, reverses sign. It is easy to show [37] that in this case the pressures decrease by an appreciably larger amount

$$\Delta P_r = 2\sigma'_{dyn}\frac{1-\mu}{1-2\mu}.$$

With further decrease in pressures, a plastic stage of flow again sets in (see Fig. 63).

At the fracture point, the ratio of the velocities of sound propagation in the elastic and plastic states is determined already by a quantity known to us, ν. As already indicated, the elastic unloading waves were disclosed in experiments performed in accordance with the scheme of Fig. 29. By way of illustration, the right side of Table VII shows for comparison values of "plastic" or gasdynamic velocities C_p and elastic sound velocities C_{el}, taken from [37], for aluminum, copper, and iron. In these metals the slope of the isentropes

$$\left(\frac{\partial P}{\partial \varrho}\right)_S = C^2$$

decreases by 1.35—1.40 on going into the plastic state.

Elastic waves were observed later by Eichelberger and Hauver [81] with the aid of a pickup of a new type, which fixed the arrival of the unloading wave after thin plates were made to strike a target. Under analogous conditions "non-gasdynamic" attenuation of shock waves in aluminum, due to the leading waves of elastic relaxation, were investigated by Curran [102] and others.

They first determined the amplitude of elastic relaxation in aluminum, in other words, its strength under shock compression at 220 kbar; according to [102], σ'_{dyn} = 12 kbar.

These results disclose the simultaneous effect of many factors on the strength: the deformation rate, high hydrostatic pressure, and rising temperature.

In the preceding sections, the effects of strength were assumed to be negligibly small and the crystalline bodies were regarded as being quasi-liquid and possessing the scalar pressure field characteristic of liquids.

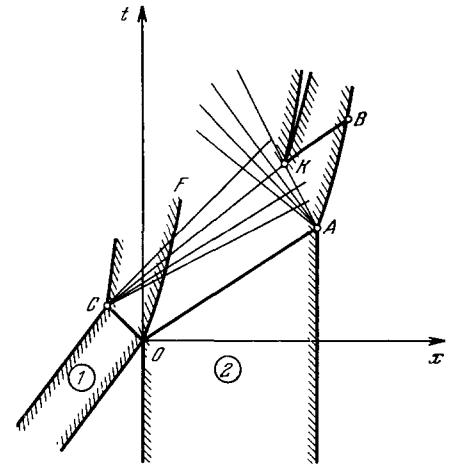

FIG. 64. x-t diagram for cleavage when a thin plate strikes a partition. 1 – Striking plate; 1 – partition; OA and OC – trajectories of shock waves; A – poles of centered relaxation waves; AK – characteristic carrying the maximum rupture stresses.

Actually, we see that the states of shock-compressed bodies are described by a stress tensor whose principal stresses differ by an amount equal to the dynamic yield point.

In a more rigorous analysis [160,163], the results of dynamic experiments show the variation of normal stresses to differ from that of hydrostatic compression by an amount $(2\sigma'_{dyn}/3)$ (see Fig. 61). The yield point σ'_{dyn} itself is not invariant, and depends not only on the deformation rate but also on the pressure and temperature.

As follows from the work of Bridgman [167] and Vereshchagin et al [9], the increase of σ_{st} with pressure under static conditions is large. On the dynamic adiabat, the increase in σ'_{dyn} upon compression is offset by its decrease with rising temperature. The true course of variation of σ'_{dyn} is not known at present. However, judging from the data of [102], the error introduced into the equations of state of the investigated substances when $P_r(v)$ is set equal to $P(v)$ is not large.

In conclusion let us stop to discuss shock-explosive destruction of materials by normal tensile stresses. The regions of negative pressures are produced when opposite rarefaction waves interact, stretching the samples in opposite directions.

The x-t diagram of Fig. 64 shows waves of this type, produced in colliding plates upon reflection of compression waves from the free surfaces. The encounter of the waves of rarefaction occurs inside the target plate.

When a detonation is reflected from a partition, the rarefaction wave follows directly the compression shock, as a result of which the interference of

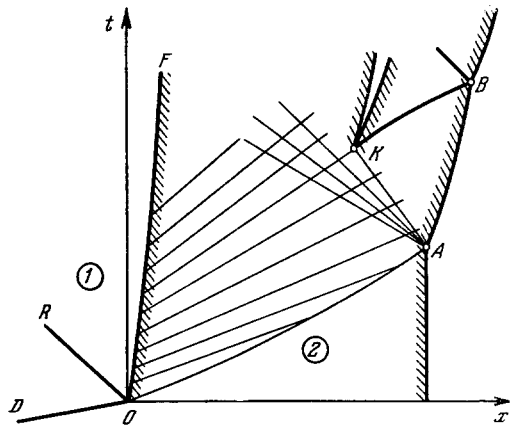

FIG. 65. x-t diagram for the cleavage when a detonation wave is reflected from a partition. 1 – region occupied by the explosion product; 2 – partition; OD – trajectory of detonation wave; OA and OR – trajectories of shock waves in the partition and in the explosive; A – pole of centered relaxation wave; AK – characteristic carrying the maximum rupture stresses.

the waves arises immediately on the free boundary of the partition (Fig. 65). In both cases the negative pressures increase as the relaxation wave penetrates inside the samples—from left to right in Figs. 64 and 65. The critical destructive stresses are usually estimated from the thickness of the cleavage platelets observed after the explosion. The destructive forces are identified in this case with the calculated tension stresses at the cleavage section.

According to Rinehart [114] who set up experiments in accordance with the scheme of Fig. 65 on plates of large thicknesses, the rupture stress for aluminum, copper, and soft steel is 9.8, 28.7 and 11.2 kbar/cm^2, respectively.

As shown by Nahami [168], the theoretical values of the rupture stresses increase with decreasing thickness of the partition. Particularly large values of rupture stresses, 120 kbar/cm, approaching the theoretical strength of copper, were obtained by McQueen and Marsh [169] in the destruction of thin copper plates in accordance with the scheme of Fig. 64. Comparison of such diverse results shows that the critical destructive stress under these conditions is not a definite characteristic of the material.

The destruction of samples by rarefaction waves is a time consuming process involving occurrence and development of cracks, the mutual intersection of which forms the cleavage surface. Therefore, the position of the cleavage surface depends both on the magnitude of the destructive stresses and on the scale of the experiment.

[1] L. D. Landau and E. M. Lifshitz, Statisticheskaya fizika (Statistical Physics), 2d. Ed., Gostekhizdat, 1951.

[2] D. A. Kirzhnits, JETP 32, 115 (1957), Soviet Phys. JETP 5, 64 (1957).

[3] N. M. Kalitkin, JETP 38, 1534 (1960), Soviet Phys. JETP 11, 1106 (1960).

[4] G. M. Gandel'man, JETP 43, 131 (1962), Soviet Phys. JETP 16, 94 (1962).

[5] Ermachenko, Zel'dovich, and Gandel'man, JETP 44, 386 (1963), Soviet Phys. JETP 17, 263 (1963).

[6] P. W. Bridgman, Proc. Amer. Acad. Arts and Sci. 74, 425 (1942).

[7] P. W. Bridgman, Proc. Amer. Acad. Arts and Sci. 76, 1 (1945).

[8] Vereshchagin, Semerchan, Popova, and Kuzin, DAN SSSR 145, 757 (1962), Soviet Phys. Doklady 7, 692 (1963).

[9] L. F. Vereshchagin and V. A. Shapochkin, FMM 9, 258 (1960).

[10] S. Mikomura and H. G. Drickamer, J. Phys. Chem. Solids 23, 451 (1962).

[11] A. S. Balchan and H. G. Drickamer, RCV Sci. Instr. 32, 308 (1961).

[12] Progress in Very High Pressure Research, New York, 1960.

[13] S. S. Kabalkina, FTT 4, 3124 (1962), Soviet Phys. Solid State 4, 2288 (1963).

[14] P. Takahashi and W. A. Bassett, Science 145 (No. 3631), 483 (1964).

[15] V. A. Tsukerman and A. I. Avdeenko, JETP 12, 185 (1942).

[16] V. A. Tsukerman, DAN SSSR 40, 267 (1943).

[17] V. A. Tsukerman, DAN SSSR 53, 323 (1946).

[18] V. A. Tsukerman and M. A. Manakova, ZhTF 27, 391 (1957), Soviet Phys. Tech. Phys. 2, 353 (1957).

[19] Zyuzin, Manakova, and Tsukerman, PTE No. 1, 84 (1958).

[20] W. Schaafs, Handb. Physik v. 30, 1957.

[21] J. J. Jacobs, ARS Journal 30(2), 151 (1960).

[22] Alentsev, Belyaev, Sobolev, and Stepanov, JETP 16, 990 (1946).

[23] F. C. Gibson et al., Bull. Amer. Phys. Soc., No. 1 (1957).

[24] I. Sh. Model', JETP 32, 714 (1957), Soviet Phys. JETP 5, 589 (1957).

[25] Zel'dovich, Kormer, Sinitsyn, and Kuryapin, DAN SSSR 122, 48 (1958), Soviet Phys. Doklady 3, 938 (1959).

[26] I. M. Voskoboĭnikov and A. Ya. Apin, DAN SSSR 130, 804 (1960).

[27] Ya. B. Zel'dovich and Yu. P. Raĭzer, Fizika udarnykh voln i vysokotemperaturnykh gidrodinamicheskikh yavleniĭ, (Physics of Shock Waves and High-temperature Hydrodynamic Phenomena), Fizmatgiz, 1963.

[28] Solid State Physics, vol. 6, Academic Press Publ., New York and London, 1958.

[29] Solids under Pressure, Ed. William Paul, Douglas M. Warschauer, New York, 1963.

[30] G. E. Duvall, Appl. Mech. Rev. 15(11), 849 (1962).

[31] R. Courant and K. O. Friedrichs, Supersonic Flow and Shock Waves, Interscience, 1948.

[32] Ya. B. Zel'dovich, Teoriya udranykh voln i vvedenie v gazodinamiku (Theory of Shock Waves and Introduction to Gasdynamics), AN SSSR, 1946.
[33] Baum, Stanyukovich, and Shekhter, Fizika vzryva (Explosion Physics), Fizmatgiz, 1959.
[34] C. Kittell, Introduction to Solid State Physics, Wiley, 1953.
[35] Ya. B. Zel'dovich, JETP 32, 1577 (1957), Soviet Phys. JETP 5, 1287 (1957).
[36] Al'tshuler, Krupnikov, Ledenev, Zhuchikhin, and Brashnik, JETP 34, 874 (1958), Soviet Phys. JETP 7, 606 (1958).
[37] Al'tshuler, Kormer, Brazhnik, Vladimirov, Speranskaya, and Funtikov, JETP 38, 1061 (1960), Soviet Phys. JETP 11, 766 (1960).
[38] Al'tshuler, Krupnikov, and Brazhnik, JETP 34, 886 (1958), Soviet Phys. JETP 7, 614 (1958).
[39] Al'tshuler, Kormer, Bakanova, and Trunin, JETP 38, 790 (1960), Soviet Phys. JETP 11, 573 (1960).
[40] R. G. McQueen and S. P. Marsh, J. Appl. Phys. 31, 1253 (1960).
[41] C. Skidmore and E. Morris, Proceedings of Symposium, Vienna, May 1962.
[42] Al'tshuler, Bakanova, and Trunin, JETP 42, 91 (1962), Soviet Phys. JETP 15, 65 (1962).
[43] Krupnikov, Bakanova, Brazhnik, and Trunin, DAN SSSR 148, 1302 (1963), Soviet Phys. Doklady 8, 203 (1963).
[44] Goranson, Bancroft, Burton, Blechar, Houston, Gittings, and Landeen, J. Appl. Phys. 26, 555 (1955).
[45] M. D. Mallory, J. Appl. Phys. 26, 555 (1955).
[46] Shirman, Dubovik, and Kevlishvili, Sverkhskorostnaya fotoregistriruyushchaya ustanovka SFR (SFR super high speed photocamera), AN SSSR, 1957.
[47] J. M. Walsh and R. H. Christian, Phys. Rev. 97, 1544 (1955).
[48] I. C. Slater, Introduction to Chemical Physics, New York—London, 1939.
[49] L. D. Landau and K. P. Stanyukovich, DAN SSSR 46, 399 (1945).
[50] I. S. Dugdall and D. McDonald, Phys. Rev. 89, 832 (1953).
[51] V. N. Zubarev and V. Ya. Vashchenko, FTT 5, 886 (1963), Soviet Phys. Solid State 5, 653 (1963).
[52] Hirschfelder, Curtiss, and Bird, Molecular Theory of Gases and Liquids, Wiley, 1954.
[53] Al'tshuler, Pavlovskii, Kuleshova, and Simakov, FTT 5, 279 (1963), Soviet Phys. Solid State 5, 203 (1963).
[54] Kormer, Funtikov, Urlin, and Kolesnikova, JETP 42, 686 (1962), Soviet Phys. JETP 15, 477 (1962).
[55] Kormer, Sinitsyn, Funtikov, Urlin, and Blinov, JETP 47, 1202 (1964), Soviet Phys. JETP 20, 811 (1965).
[56] V. N. Zubarev and G. S. Telegin, DAN SSSR 142, 309 (1962), Soviet Phys. Doklady 7, 34 (1962).
[57] V. N. Zubarev and G. S. Telegin, DAN SSSR 147, 1122 (1962).
[58] V. N. Zubarev and G. S. Telegin, DAN SSSR 158, 452 (1964), Soviet Phys. Doklady 9, 819 (1965).
[59] B. J. Alder and M. Van Thiel, Phys. Letts. 1(5), 317 (1963).
[60] S. B. Kormer, Urlin, and Popova, FTT 3, 2131 (1961), Soviet Phys. Solid State 3, 1547 (1962).
[61] S. B. Kormer and V. D. Urlin, DAN SSSR 131, 542 (1960), Soviet Phys. Doklady 5, 317 (1960).
[62] V. N. Zharkov and V. A. Kalinin, DAN SSSR 135, 811 (1960), Soviet Phys. Doklady 5, 1253 (1961).
[63] Al'tshuler, Kuleshova, and Pavlovskiĭ, JETP 39, 16 (1960), Soviet Phys. JETP 12, 10 (1961).
[64] M. Born and K. Huang, Dynamical Theory of Crystal Lattices, Oxford, 1954.
[65] V. D. Urlin and A. A. Ivanov, DAN SSSR 149, 1303 (1963), Soviet Phys. Doklady 8, 380 (1963).
[66] B. I. Davidov, Izv. AN SSSR ser. geofiz. No. 12 (1965).
[67] D. L. Chapman, Phil. Mag. 47, 90 (1899).
[68] E. Jouget, Mechaniques des explosifs, O. Doin et Fils, Paris, 1917.
[69] Ya. B. Zel'dovich, JETP 10, 542 (1940).
[70] J. Neumann, OSRD, No. 549 (1942).
[71] J. Teylor, Detonation in Condensed Explosives, Clarendon Press, Oxford, 1952.
[72] K. P. Stanyukovich and T. I. Pokrovskiĭ, Izv. AN SSSR 8(4), 214 (1944).
[73] A. Schmidt, Zs. Ges., Schiess und Sprengstoffwessen 30, 364 (1935).
[74] W. E. Deal, Phys. Fluids 1(6), 523 (1958).
[75] W. E. Deal, J. Chem. Phys. 27, 796 (1957).
[76] A. N. Dremin and G. A. Adadurov, Izv. AN SSSR, OKhN, No. 6, 1130 (1960).
[77] A. N. Dremin and P. F. Pokhil, DAN SSSR 128, 989 (1959).
[78] A. N. Dremin and K. K. Shvedov, PMTF, No. 2, 154 (1964).
[79] R. E. Duff and E. E. Houston, J. Chem. Phys. 23, 1268 (1955).
[80] A. N. Dremin and P. F. Pokhil, ZhFKh 34, 2561 (1960).
[81] R. I. Eichelberger and G. E. Hauver, in Coll. Les ondes de detonation, Paris, 1961, p. 364.
[82] A. N. Dremin and O. K. Rozanov, DAN SSSR 139, 137 (1961).
[83] Zel'dovich, Kormer, Krishkevich, and Yushko, DAN SSSR 158, 1058 (1964), Soviet Phys. Doklady 9, 857 (1965).
[84] V. A. Tsukerman and A. A. Brish, Letter to the Editor, PMFT, in press.
[85] Zaĭtsev, Pokhil, and Shvedov, DAN SSSR 132, 1339 (1960).
[86] V. N. Zubarev, PMFT, No. 2, (1965).
[87] J. M. Walsh and M. H. Rice, J. Chem. Phys. 26(4), 815 (1957).

[88] M. H. Rice and J. M. Walsh, J. Chem. Phys. 26(4), 824 (1957).
[89] Al'tshuler, Bakanova, and Trunin, DAN SSSR 121, 67 (1958), Soviet Phys. Doklady 3, 761 (1959).
[90] R. O. Cowan and W. Fickett, J. Chem. Phys. 24(5), 932 (1956).
[91] Dremin, Koldunov, and Shvedov, PMTF 6, 131 (1963).
[92] Walsh, Rice, McQueen, and Jarger, Phys. Rev. 108(2), 196 (1957).
[93] Bakanova, Trunin, and Dudoladov, FTT 7, No. 6 (1965).
[94] Krupnikov, Brazhnik, and Krupnikova, JETP 42, 675 (1962), Soviet Phys. JETP 15, 470 (1962).
[95] J. I. Gilvary, Phys. Rev. 96, 934, 944 (1954); 102, 317 (1956).
[96] J. I. Gilvary and G. H. Reebles, Phys. Rev. 99, 550 (1955).
[97] R. Latter, Phys. Rev. 99, 1854 (1955).
[98] K. Anders, Phys. Letts. 7(5) (1963).
[99] G. K. White, Phil. Mag. 6(66) (1961).
[100] I. M. Lifshitz, JETP 38, 1569 (1960), Soviet Phys. JETP 11, 1130 (1960).
[101] G. R. Fowles, J. Appl. Phys. 31, (4) (1960).
[102] D. R. Curran, J. Appl. Phys. 34(9), 2677 (1963).
[103] Barker, Lundergan, and Herrman, J. Appl. Phys. 35(4), 1203 (1964).
[104] Al'tshuler, Tarasov, and Speranskaya, FMM 13, 738 (1962).
[105] Jean Jacquesson, Contribution a l'etude de la propagation et des effects des ondes de choc dans les metaux, De l'universite de Portiers, 1962.
[106] L. V. Al'tshuler and A. P. Petrunin, ZhTF 31, 717 (1960), Soviet Phys. Tech. Phys. 6, 516 (1961).
[107] G. A. Feoktistova, DAN SSSR 136, 1325 (1961), Soviet Phys. Doklady 6, 162 (1961).
[108] Al'tshuler, Kormer, Bakanova, Petrunin, Funtikov, and Gubkin, JETP 41, 1382 (1961), Soviet Phys. JETP 14, 986 (1962).
[109] R. J. Seeger and H. Polacher, J. Appl. Phys. 22(5), 640 (1951).
[110] Bancroft, Peterson, and Minshall, J. Appl. Phys. 27, 291 (1956).
[111] R. E. Duff and F. S. Minshall, Phys. Rev. 108, 1207 (1957).
[112] J. Wackerle, J. Appl. Phys. 33(3), 922 (1962).
[113] Novikov, Divnov, and Ivanov, JETP 47, 814 (1964), Soviet Phys. JETP 20, 545 (1965).
[114] I. S. Rinehart and J. Pearson, Behavior of Metals under Impulsive Loads, ASM, Cleveland, 1954.
[115] Response of Metals to High Velocity Deformation, Interscience, 1960.
[116] A. G. Ivanov and S. A. Novikov, PTE 1, No. 7, 135 (1963).
[117] Johnson, Stein, and Davis, J. Appl. Phys. 33(2), 557 (1962).
[118] J. C. Jamieson and A. W. Lawson, J. Appl. Phys. 33(3) (1963).
[119] A. G. Ivanov and S. A. Novikov, JETP 40, 1880 (1961), Soviet Phys. JETP 13, 1321 (1961).
[120] A. G. Ivanov, Novikov, and Tarasov, FTT 4, 249 (1962), Soviet Phys. Solid State 4, 177 (1962).
[121] J. O. Erkman, J. Appl. Phys. 32, 939 (1961).
[122] A. S. Balchan, J. Appl. Phys. 34, 241 (1963).
[123] W. E. Drummond, J. Appl. Phys. 28, 999 (1957).
[124] Perez-Albuerne, Forsgren, and Drickamer, Rev. Sci. Instrum. 35, (1), 29 (1964).
[125] Pavlovskii, Vashchenko, and Simakov, FTT 7, No. 4, 1965.
[126] Brish, Tsukerman, and Tarasov, JETP 37, 1543 (1959), Soviet Phys. JETP 10, 1095 (1960).
[127] B. J. Alder and R. H. Christian, Phys. Rev. 104, 550 (1956).
[128] P. O. Lövdin, A. Theoretical Investigation into Some Properties of Ionic Crystals, Uppsala, 1948.
[129] V. V. Evdokimova and L. F. Vereshchagin, FTT 4, 1065 (1962), Soviet Phys. Solid State 4, 784 (1962).
[130] V. V. Evdokimova and L. F. Vereshchagin, JETP 43, 1208 (1962), Soviet Phys. JETP 16, 855 (1963).
[131] M. Flower and N. U. March, Phys. Rev. 125, 1144 (1962).
[132] V. P. Trubitsin and F. R. Ulinich, in coll. Tverdoe telo v usloviyakh davleniĭ i temperatur zemnykh nedr (Solids Under the Pressure and Temperature Conditions of the Earth's Interior), AN SSSR, 1964; Izv. AN SSSR ser. Geofiz. No. 6, 949 (1963).
[133] A. A. Abrikosov, Astron. zh. 31, 112 (1954).
[134] B. J. Alder and R. H. Christian, Phys. Rev. Letts. 4, 450 (1960).
[135] R. H. Bube, Photoconductivity of Solids, Wiley, 1960.
[136] G. M. Gandel'man, JETP 48, No. 6, 1965. Soviet Phys. JETP 21, No. 6 (1965).
[137] J. C. Jamieson, Science 139 (No. 3556), 46 (1960).
[138] R. H. Wentorf and I. S. Kasper, Science 139 (No. 3552), 338 (1963).
[139] B. J. Alder and R. H. Christian, Phys. Rev. Letts. 7, 367 (1961).
[140] P. S. DeCarbi and J. C. Jamieson, Science 133 (no. 3467), 1821 (1961).
[141] W. E. Libby, Proc. Nat. Acad. Sci. USA, No. 9, 1475 (1962).
[142] F. Birch, Geophys. J. (London) 4, 295 (1961).
[143] A. E. Ringwood, J. Geophys. Res. 67(10), 4005 (1962).
[144] S. M. Stishov, Geokhimiya, No. 8, 649 (1962).
[145] S. M. Stishov and S. V. Popova, ibid. 10, 837 (1961).
[146] D. S. Hughes and R. G. McQueen, Trans. Amer. Geophys. Union 39(5), 259 (1958).
[147] L. V. Al'tshuler and S. B. Kormer, Izv. AN SSSR ser. geofiz. No. 1, 3 (1961).
[148] S. B. Kormer and A. I. Funtikov, Izv. AN SSSR, ser. Fiz. Zemli (Earth Physics Series), (1965).

[149] V. N. Lodochnikov, Zap. Vseross. mineral. o-va (Notes of the All-Russian Mineral Society), Ser. 2, part 64, 207 and 428 (1939).

[150] W. H. Ramsey, Month. Not. Roy. Arts. Soc. 108, 406 (1948).

[151] B. Yu. Levin, In coll. Voprosy vnutrennego stroyeniya i razvitiya Zemli (Problems of the Internal Structure and Development of the Earth). Trudy, Geophys. Inst. Acad. Sci., No. 26, 208 (153) (1955); Mem. Soc. Sci. Liege 24, 39 (1962).

[152] V. N. Zharkov, Trudy, Earth Physics Inst. Acad. Sci. No. 20, 3 (1962); DAN SSSR 135, 1378 (1960).

[153] L. Knopoff and G. J. F. Macdonald, Sci. New. Letts., No. 75.

[154] C. S. Smith, Memorial de l'artillerie traciaise 35(136), 463 (1961).

[155] Pock, Evans, and James, Proc. Phys. Soc. 60 (337), 1 (1948).

[156] M. A. Allen and C. A. McGrary, Rev. Sci. Instr. 24, 165 (1953).

[157] S. Minshall, J. Appl. Phys. 26, 463 (1955).

[158] E. Costello, The Tust. Mech. Engng. Proc. of the Conference on Properties of Material at High Rates of Strain (London, 1957), 1958, p. 13.

[159] Ivanov, Novikov, and Sinitsyn, FTT 5, 269 (1963), Soviet Phys. Solid State 5, 196 (1963).

[160] G. R. Fowles, J. Appl. Phys. 32, 1475 (1961).

[161] J. W. Taylor and M. H. Rice, J. Appl. Phys. 34, 364 (1963).

[162] Jones, Nellson, and Benedick, J. Appl. Phys. 33, 3224 (1962).

[163] Jean Jacquesson, in coll. Les ondes de detonation, Paris, 1961.

[164] G. E. Duvall, in coll. Les ondes de detonation, Paris, 1961, p. 337.

[165] G. I. Barenblatt, PMM 17, 455 (1953).

[166] A. N. Dremin and G. A. Adadurov, FTT 6, 1757 (1964), Soviet Phys. Solid State 6, 1379 (1964).

[167] P. W. Bridgman, Investigation of Large Plastic Deformations and Rupture (Russ. Transl.) IIL, 1955.

[168] G. Nahami, in coll. Les ondes de detonation, Paris, 1961, p. 451.

[169] R. G. McQueen and S. P. March, J. Appl. Phys. 33(2), 654 (1962).

Translated by J. G. Adashko